AWARD NUMBER: W81XWH-16-1-0595

TITLE: Prostate-specific Membrane Antigen (PSMA) Targeted Bioorthogonal Therapy for Metastatic Prostate Cancer

PRINCIPAL INVESTIGATOR: D. Artemov., Ph.D.

CONTRACTING ORGANIZATION: Johns Hopkins University
School of Medicine
Baltimore, MD, 21205-2196

REPORT DATE: Jan 2021

TYPE OF REPORT: Final

PREPARED FOR: U.S. Army Medical Research and Development Command
Fort Detrick, Maryland 21702-5012

REPORT DOCUMENTATION PAGE

Form Approved
OMB No. 0704-0188

1. REPORT DATE	2. REPORT TYPE	3. DATES COVERED
Jan 2021	Final	09/15/2016 - 09/14/2020

4. TITLE AND SUBTITLE

Prostate-specific Membrane Antigen (PSMA) Targeted Bioorthogonal Therapy for Metastatic Prostate Cancer

5a. CONTRACT NUMBER

5b. GRANT NUMBER
W81XWH-16-1-0595

5c. PROGRAM ELEMENT NUMBER

6. AUTHOR(S)

D. Artemov, Ph.D.

E-Mail: dartemo2@jh.edu

5d. PROJECT NUMBER

5e. TASK NUMBER

5f. WORK UNIT NUMBER

7. PERFORMING ORGANIZATION NAME(S) AND ADDRESS(ES)

Johns Hopkins University School of Medicine Baltimore, MD,

21205-2196

8. PERFORMING ORGANIZATION REPORT NUMBER

9. SPONSORING / MONITORING AGENCY NAME(S) AND ADDRESS(ES)

U.S. Army Medical Research and Development Command
Fort Detrick, Maryland 21702-5012

10. SPONSOR/MONITOR'S ACRONYM(S)

11. SPONSOR/MONITOR'S REPORT NUMBER(S)

12. DISTRIBUTION / AVAILABILITY STATEMENT

Approved for Public Release; Distribution Unlimited

13. SUPPLEMENTARY NOTES

14. ABSTRACT

During the final year of the project we have tested and validated pretargeting delivery of mertansine drug carriers to prostate cancer using 5D3 monoclonal antibody and compared it with Fab2 fragments. *In vitro* studies in cultured prostate cancer cells has been completed and a paper was published in *Molecular Pharmaceutics*. Quantitative analysis of cell images allowed measurement of internalization rates of different pretargeting agent and drug carriers. Kinetics of internalization plays important role in the pretargeting concept, as the pretargeting component should be available on surface of targeted cells at the time of administration of the drug carrier component. For *in vivo* applications new pretargeting click-reactive components are needed and we have identified a 5D3 antibody fragment that retain extremely high PSMA binding affinity and has relatively long life-time on the cell surface before internalization, comparable with its *in vivo* pharmacokinetics. PET/MR imaging of PSMA pretargeting in prostate cancer models have been performed and suggested excellent physiological profile of the new system.

15. SUBJECT TERMS					
16. SECURITY CLASSIFICATION OF:			17. LIMITATION OF ABSTRACT	18. NUMBER OF PAGES	19a. NAME OF RESPONSIBLE PERSON USAMRMC
a. REPORT Unclassified	b. ABSTRACT Unclassified	c. THIS PAGE Unclassified	Unclassified	38	19b. TELEPHONE NUMBER *(include area code)*

Standard Form 298 (Rev. 8-98)
Prescribed by ANSI Std. Z39.18

An abstract shall be provided in Block 14 and shall state the purpose, scope, and major findings and be an up-to-date report of the progress in terms of results and significance. Abstracts will be submitted to the Defense Technical Information Center (DTIC) and shall not contain proprietary information. Subject terms are keywords that may have been previously assigned to the proposal abstract or are keywords that may be significant to the research.

TABLE OF CONTENTS

1. **INTRODUCTION:** *Narrative that briefly (one paragraph) describes the subject, purpose and scope of the research.*

In this application, we propose to develop and validate a novel, two-component, targeted therapeutic system that will provide a safe and precise way to deliver toxic anticancer drugs directly to tumor cells and minimize toxic effects for patients. This goal will be achieved by highly PSMA-specific pretargeting agents followed by cytotoxic drug carriers, with optimized pharmacokinetics and clearance. A new ligation click chemistry that does not interfere with any known biological functions is used for *in situ* conjugation. Both components of the delivery system can be tracked by imaging to enable monitoring of PSMA status, and to optimize treatment schedule during therapy.

2. **KEYWORDS:** *Provide a brief list of keywords (limit to 20 words).*

Anti-PSMA monoclonal antibody, targeted therapy, *in vivo* imaging, antibody internalization, cytotoxic conjugates, two-component therapy, pretargeting

3. **ACCOMPLISHMENTS:** *The PI is reminded that the recipient organization is required to obtain prior written approval from the awarding agency grants official whenever there are significant changes in the project or its direction.*

What were the major goals of the project?

List the major goals of the project as stated in the approved SOW. If the application listed milestones/target dates for important activities or phases of the project, identify these dates and show actual completion dates or the percentage of completion.

In this application, we propose to develop and validate a novel, two-component, PSMA-targeted therapeutic system that will provide a safe and precise way to deliver toxic anticancer drugs directly to prostate cancer tumor cells and minimize toxic effects for patients. To achieve this goal PSMA pretargeting using a new ligation chemistry is used, thus limiting the circulation time of cytotoxic drug carriers.

The therapy includes two components that are administered within a specific interval of 12-24h. The first component is PSMA-pretargeting agent, and the second component delivers DM1 anticancer drugs to cells pre-labeled with the first component. Both components of the delivery system can be noninvasively imaged during the treatment.

The new therapeutic strategy is to be initially tested in prostate cancer cells, and then *in vivo* in mouse models of human metastatic prostate cancer. Our aspiration is that, if successful, this treatment strategy can be used to treat advanced and metastatic PSMA-positive prostate cancer with high efficacy and minimal systemic toxicity.

What was accomplished under these goals?

For this reporting period describe: 1) major activities; 2) specific objectives; 3) significant results or key outcomes, including major findings, developments, or conclusions (both positive and negative); and/or 4) other achievements. Include a discussion of stated goals not met. Description shall include pertinent data and graphs in sufficient detail to explain any significant results achieved. A succinct description of the methodology used shall be provided. As the project progresses to completion, the emphasis in reporting in this section should shift from reporting activities to reporting accomplishments.

1. We have synthesized and characterized the following pretargeting agents:

(i) Functionalized 5D3 anti-PSMA monoclonal antibody with TCO functional group for click-chemistry conjugation and green AF488 fluorophore for microscopy.

(ii) Functionalized 5D3 anti-PSMA monoclonal antibody with TCO functional group for click-chemistry conjugation and AF488 and pH-sensitive pHrodo (bright red at acidic pH) fluorophores.

(iii) Functionalized $F(ab')_2$ domain of 5D3 mAb with TCO and AF488 fluorophore.

(iv) Finctionalized Fab domain of 5D3 mAb with TCO and CF680 for *in vivo* and *in vitro* imaging.

(v) Finctionalized Fab domain of 5D3 mAb with TCO and ^{89}ZrDFO for PET imaging.

2. We've synthesized and characterize new cytotoxic carrier component based on human albumin conjugated with PEG-tetrazine (reactive group for click chemistry), and potent microtubule inhibitor mertansine (DM1). Modification ratios were optimized to provide high stability, high cytotoxicity, and good water solubility of the compound.

3. We have measured internalization kinetics and intracellular distribution of internalized components in PSMA+ human prostate cancer cells. Specific cytotoxic effect against PSMA-expressing cells was confirmed; results are summarized in our publication in Hapuarachchige et al. *Molecular Pharmaceutics*, 2020.

4. Based on extremely high affinity and internalization rates of 5D3 anti-PSMA mAb we have synthesized a direct 5D3-DM1 antibody-drug conjugates and tested there anticancer effects in cultures prostate cancer cells and in preclinical models of human prostate cancer. Excellent localization of the drug in pSMA-expressing tumors was detected by optical imaging (Fig .1A). High efficacy of the agent against PSMA-expressing cancer and low to negligible systemic toxicity in small animals were confirmed. Results are summarized in a paper Huang et al., *Molecular Pharmaceutics*, 2020.

5. PET imaging of Fab-based pretargeting agents was performed in animal models of PSMA-positive and PSMA-negative prostate cancer using long lived 89-zirconium tracer. Results presented in Fig. 1 and demonstrate feasibility of this agent for future application in pretargeting therapy.

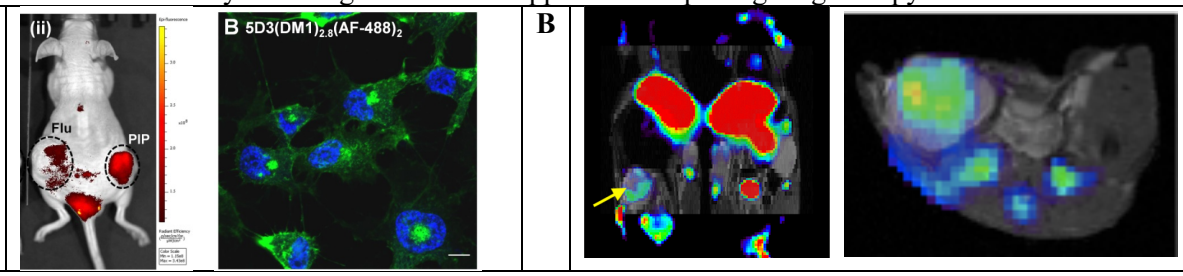

Figure 1. **A**. Tumor uptake of $5D3(DM1)_{2.8}(CF\text{-}680)_2$ in PSMA(+) PC3-PIP and PSMA(-) PC3-Flu dual tumor mouse model. $5D3(DM1)_{2.8}(AF\text{-}488)_2$ comletely internalized in PC3-PIP cells after 1h. **B**. PET-MRI at 7T shows distribution of 89Zr PET radiotracer with MR image**.** MRI: RARE pulse sequence (in plane resolution of 0.25 mm; slice thickness of 1 mm; TE/TR= 36/3000ms). PET: 15 min scan was performed 24h after injection of 210 μCi of ^{89}Zr-Fab of anti-PSMA 5D3 mAb. Reconstructed spatial resolution of 0.75mm. PSMA+ PC3-PIP tumor in the left flank (yellow arrow) shows high uptake of the radiotracer. No uptake was detected in PSMA- tumor (right mouse). High uptake in the liver was also observed.

What opportunities for training and professional development has the project provided?
If the project was not intended to provide training and professional development opportunities or there is nothing significant to report during this reporting period, state "Nothing to Report."

Describe opportunities for training and professional development provided to anyone who worked on the project or anyone who was involved in the activities supported by the project. "Training" activities are those in which individuals with advanced professional skills and experience assist others in attaining greater proficiency. Training activities may include, for example, courses or one-on-one work with a mentor. "Professional development" activities result in increased knowledge or skill in one's area of expertise and may include workshops, conferences, seminars, study groups, and individual study. Include participation in conferences, workshops, and seminars not listed under major activities.

Nothing to Report

How were the results disseminated to communities of interest?
If there is nothing significant to report during this reporting period, state "Nothing to Report."

Describe how the results were disseminated to communities of interest. Include any outreach activities that were undertaken to reach members of communities who are not usually aware of these project activities, for the purpose of enhancing public understanding and increasing interest in learning and careers in science, technology, and the humanities.

Nothing to Report

Describe briefly what you plan to do during the next reporting period to accomplish the goals and objectives.

Nothing to Report – this is the Final Report

4. **IMPACT:** D*escribe distinctive contributions, major accomplishments, innovations, successes, or any change in practice or behavior that has come about as a result of the project relative to:*

What was the impact on the development of the principal discipline(s) of the project?
If there is nothing significant to report during this reporting period, state "Nothing to Report."

Describe how findings, results, techniques that were developed or extended, or other products from the project made an impact or are likely to make an impact on the base of knowledge, theory, and research in the principal disciplinary field(s) of the project. Summarize using language that an intelligent lay audience can understand (Scientific American style).

Novel two-component pretargeting system for specific therapy of PSMA-expressing prostate cancer can result in high efficacy and significantly reduced toxicity and side effects. Our improved therapeutic components (pretargeting and drug-carrier) provide favorable pharmacokinetics and internalization kinetics in target cancer cells, which should facilitate experimental therapy in animal models. Once optimized and validated future translation to clinic should be feasible.

What was the impact on other disciplines?
If there is nothing significant to report during this reporting period, state "Nothing to Report."

Describe how the findings, results, or techniques that were developed or improved, or other products from the project made an impact or are likely to make an impact on other disciplines.

The developed pretargeting system can impact on specific diagnostic imaging of prostate cancer using retargeting probes for improved sensitivity and specificity of detection and ability to use a combination of high-molecular weight targeting molecules (antibodies or engineered antibody fragments) with short life-time small-molecule imaging probes.

What was the impact on technology transfer?
If there is nothing significant to report during this reporting period, state "Nothing to Report."

Describe ways in which the project made an impact, or is likely to make an impact, on commercial technology or public use, including:

- *transfer of results to entities in government or industry;*
- *instances where the research has led to the initiation of a start-up company; or*
- *adoption of new practices.*

Nothing to Report

What was the impact on society beyond science and technology?
If there is nothing significant to report during this reporting period, state "Nothing to Report."

Describe how results from the project made an impact, or are likely to make an impact, beyond the bounds of science, engineering, and the academic world on areas such as:

- *improving public knowledge, attitudes, skills, and abilities;*
- *changing behavior, practices, decision making, policies (including regulatory policies), or social actions; or*
- *improving social, economic, civic, or environmental conditions.*

Nothing to Report

5. CHANGES/PROBLEMS: *The PD/PI is reminded that the recipient organization is required to obtain prior written approval from the awarding agency grants official whenever there are significant changes in the project or its direction. If not previously reported in writing, provide the following additional information or state, "Nothing to Report," if applicable:*

Nothing to Report

Describe problems or delays encountered during the reporting period and actions or plans to resolve them.

Nothing to Report

Changes that had a significant impact on expenditures

Describe changes during the reporting period that may have had a significant impact on expenditures, for example, delays in hiring staff or favorable developments that enable meeting objectives at less cost than anticipated.

Nothing to Report

Significant changes in use or care of human subjects, vertebrate animals, biohazards, and/or select agents

Describe significant deviations, unexpected outcomes, or changes in approved protocols for the use or care of human subjects, vertebrate animals, biohazards, and/or select agents during the reporting period. If required, were these changes approved by the applicable institution committee (or equivalent) and reported to the agency? Also specify the applicable Institutional Review Board/Institutional Animal Care and Use Committee approval dates.

Significant changes in use or care of human subjects

Not Applicable – Nothing to Report

Significant changes in use or care of vertebrate animals

Nothing to Report

Significant changes in use of biohazards and/or select agents

Nothing to report

6. **PRODUCTS:** *List any products resulting from the project during the reporting period. If there is nothing to report under a particular item, state "Nothing to Report."*

- **Publications, conference papers, and presentations**
  Report only the major publication(s) resulting from the work under this award.

Journal publications. *List peer-reviewed articles or papers appearing in scientific, technical, or professional journals. Identify for each publication: Author(s); title; journal; volume: year; page numbers; status of publication (published; accepted, awaiting publication; submitted, under review; other); acknowledgement of federal support (yes/no).*

1. Huang CT, Guo X, Bařinka C, Lupold SE, Pomper MG, Gabrielson K, Raman V, Artemov D, Hapuarachchige S. Development of 5D3-DM1: A Novel Anti-Prostate-Specific Membrane Antigen Antibody-Drug Conjugate for PSMA-Positive Prostate Cancer Therapy. Mol Pharm. 2020 Sep 8;17(9):3392-3402.
2. Hapuarachchige S, Huang CT, Donnelly MC, Bařinka C, Lupold SE, Pomper MG, Artemov D. Cellular Delivery of Bioorthogonal Pretargeting Therapeutics in PSMA-Positive Prostate Cancer. Mol Pharm. 2020 Jan 6;17(1):98-108.
3. Hapuarachchige S, Artemov D. Theranostic Pretargeting Drug Delivery and Imaging Platforms in Cancer Precision Medicine. Front Oncol. 2020 Jul 22;10:1131.

Books or other non-periodical, one-time publications. *Report any book, monograph, dissertation, abstract, or the like published as or in a separate publication, rather than a periodical or series. Include any significant publication in the proceedings of a one-time conference or in the report of a one-time study, commission, or the like. Identify for each one-time publication: author(s); title; editor; title of collection, if applicable; bibliographic information; year; type of publication (e.g., book, thesis or dissertation); status of publication (published; accepted, awaiting publication; submitted, under review; other); acknowledgement of federal support (yes/no).*

Nothing to report

tion as noted above. List presentations made during the last year (international, national, local societies, military meetings, etc.). Use an asterisk (*) if presentation produced a manuscript.

1. S Hapuarachchige, C Huang, J Flores, C Barinka, D Artemov. "MR and optical imaging study to evaluate effects on bioorthogonal click therapy in prostate cancer mouse models", ISMRM Annual Meeting Proceedings, 3593, Paris (2018).
2. D. Artemov "Treatment Monitoring Using Smart MRI Agents", Educational Course Theranostics & Novel Molecular Probes, ISMRM Annual Meeting, Paris (2018).
3. S Hapuarachchige, RC Mease, W Lesniak, CT Huang, G Si, D Artemov. WMIC Annual Meeting Proceedings, GA138, Montreal (2019).

- **Website(s) or other Internet site(s)**
  List the URL for any Internet site(s) that disseminates the results of the research activities. A short description of each site should be provided. It is not necessary to include the publications already specified above in this section.

hopkinsmedicine.org/radiology/research/divisions/cancer-imaging-research

this is a general site for the Division of Cancer Imaging Research at the Department of Radiology and Radiological Science at JHU School of Medicine.

- **Technologies or techniques**
  Identify technologies or techniques that resulted from the research activities. Describe the technologies or techniques were shared.

Nothing to report

-
- **Inventions, patent applications, and/or licenses**
  Identify inventions, patent applications with date, and/or licenses that have resulted from the research. Submission of this information as part of an interim research performance progress report is not a substitute for any other invention reporting required under the terms and conditions of an award.

Nothing to report

- **Other Products**
  Identify any other reportable outcomes that were developed under this project. Reportable outcomes are defined as a research result that is or relates to a product, scientific advance, or research tool that makes a meaningful contribution toward the understanding, prevention, diagnosis, prognosis, treatment and /or rehabilitation of a disease, injury or condition, or to improve the quality of life. Examples include:
  - *data or databases;*
  - *physical collections;*
  - *audio or video products;*
  - *software;*
  - *models;*
  - *educational aids or curricula;*
  - *instruments or equipment;*

- *research material (e.g., Germplasm; cell lines, DNA probes, animal models);*
- *clinical interventions;*
- *new business creation; and*
- *other.*

PSMA-pretargeting system based on anti-PSMA 5D3 mAb and its fragments for specific imaging g/therapy of prostate cancer.

7. PARTICIPANTS & OTHER COLLABORATING ORGANIZATIONS

What individuals have worked on the project?

Provide the following information for: (1) PDs/PIs; and (2) each person who has worked at least one person month per year on the project during the reporting period, regardless of the source of compensation (a person month equals approximately 160 hours of effort). If information is unchanged from a previous submission, provide the name only and indicate "no change".

Example:

Name: *Mary Smith*
Project Role: *Graduate Student*
Researcher Identifier (e.g. ORCID ID): *1234567*
Nearest person month worked: *5*

Contribution to Project: *Ms. Smith has performed work in the area of combined error-control and constrained coding.*
Funding Support: *The Ford Foundation (Complete only if the funding support is provided from other than this award.)*

Name: Dmitri Artemov
Project Role: PI
Research Identifies: dmitri
Nearest person months worked: 3
Contribution to Project: *In vivo* imaging, data interpretation, providing overall guidance to the project
Funding Support: NIH/NCI, NIH/NIBIB

Name: Sudath Hapuarachchige
Project Role: co-investigator
Research Identifies: shapuar1
Nearest person months worked: 3
Contribution to Project: Chemical synthesis and characterization of therapeutic components, *in vivo* imaging
Funding Support: NIH/NCI

Name: Colin Huang
Project Role: technician
Research Identifies:
Nearest person months worked: 6
Contribution to Project: Maintaining cell cultures, performing routine tests, confocal microscopy and image processing
Funding Support: NIH/NCI

Has there been a change in the active other support of the PD/PI(s) or senior/key personnel since the last reporting period?
If there is nothing significant to report during this reporting period, state "Nothing to Report."

If the active support has changed for the PD/PI(s) or senior/key personnel, then describe what the change has been. Changes may occur, for example, if a previously active grant has closed and/or if a previously pending grant is now active. Annotate this information so it is clear what has changed from the previous submission. Submission of other support information is not necessary for pending changes or for changes in the level of effort for active support reported previously. The awarding agency may require prior written approval if a change in active other support significantly impacts the effort on the project that is the subject of the project report.

Nothing to report

What other organizations were involved as partners?
If there is nothing significant to report during this reporting period, state "Nothing to Report."

Describe partner organizations – academic institutions, other nonprofits, industrial or commercial firms, state or local governments, schools or school systems, or other organizations (foreign or domestic) – that were involved with the project. Partner organizations may have provided financial or in-kind support, supplied facilities or equipment, collaborated in the research, exchanged personnel, or otherwise contributed.

Provide the following information for each partnership:
Organization Name:
Location of Organization: (if foreign location list country)
Partner's contribution to the project (identify one or more)

- *Financial support;*
- *In-kind support (e.g., partner makes software, computers, equipment, etc., available to project staff);*
- *Facilities (e.g., project staff use the partner's facilities for project activities);*
- *Collaboration (e.g., partner's staff work with project staff on the project);*
- *Personnel exchanges (e.g., project staff and/or partner's staff use each other's facilities, work at each other's site); and*
- *Other.*

Nothing to report

8. SPECIAL REPORTING REQUIREMENTS

COLLABORATIVE AWARDS: *For collaborative awards, independent reports are required from BOTH the Initiating Principal Investigator (PI) and the Collaborating/Partnering PI. A duplicative report is acceptable; however, tasks shall be clearly marked with the responsible PI and research site. A report shall be submitted to* ***https://ers.amedd.army.mil*** *for each unique award.*

QUAD CHARTS: *If applicable, the Quad Chart (available on https://www.usamraa.army.mil) should be updated and submitted with attachments.*

9. APPENDICES: *Attach all appendices that contain information that supplements, clarifies or supports the text. Examples include original copies of journal articles, reprints of manuscripts and abstracts, a curriculum vitae, patent applications, study questionnaires, and surveys, etc.*

Preprints

1. Huang CT, Guo X, Bařinka C, Lupold SE, Pomper MG, Gabrielson K, Raman V, Artemov D, Hapuarachchige S. Development of 5D3-DM1: A Novel Anti-Prostate-Specific Membrane Antigen Antibody-Drug Conjugate for PSMA-Positive Prostate Cancer Therapy. Mol Pharm. 2020 Sep 8;17(9):3392-3402.
2. Hapuarachchige S, Huang CT, Donnelly MC, Bařinka C, Lupold SE, Pomper MG, Artemov D. Cellular Delivery of Bioorthogonal Pretargeting Therapeutics in PSMA-Positive Prostate Cancer. Mol Pharm. 2020 Jan 6;17(1):98-108.

molecular pharmaceutics

pubs.acs.org/molecularpharmaceutics

Article

Development of 5D3-DM1: A Novel Anti-Prostate-Specific Membrane Antigen Antibody-Drug Conjugate for PSMA-Positive Prostate Cancer Therapy

Colin T. Huang, Xin Guo, Cyril Bařinka, Shawn E. Lupold, Martin G. Pomper, Kathleen Gabrielson, Venu Raman, Dmitri Artemov, and Sudath Hapuarachchige*

Cite This: *Mol. Pharmaceutics* 2020, 17, 3392−3402

Read Online

ACCESS | Metrics & More | Article Recommendations | Supporting Information

ABSTRACT: Prostate cancer (PC) is a potentially high-risk disease and the most common cancer in American men. It is a leading cause of cancer-related deaths in men in the US, second only to lung and bronchus cancer. Advanced and metastatic PC is initially treated with androgen deprivation therapy (ADT), but nearly all cases eventually progress to castrate-resistant prostate cancer (CRPC). CRPC is incurable in the metastatic stage but can be slowed by some conventional chemotherapeutics and second-generation ADT, such as enzalutamide and abiraterone. Therefore, novel therapeutic strategies are urgently needed. Prostate-specific membrane antigen (PSMA) is overexpressed in almost all aggressive PCs. PSMA is widely used as a target for PC imaging and drug delivery. Anti-PSMA monoclonal antibodies (mAbs) have been developed as bioligands for diagnostic imaging and targeted PC therapy. However, these mAbs are successfully used in PC imaging and only a few have gone beyond phase-I for targeted therapy. The 5D3 mAb is a novel, high-affinity, and fast-internalizing anti-PSMA antibody. Importantly, 5D3 mAb demonstrates a unique pattern of cellular localization to the centrosome after internalization in PSMA(+) PC3-PIP cells. These characteristics make 5D3 mAb an ideal bioligand to deliver tubulin inhibitors, such as mertansine, to the cell centrosome, leading to mitotic arrest and elimination of dividing PC cells. We have successfully developed a 5D3 mAb- and mertansine (DM1)-based antibody-drug conjugate (ADC) and evaluated it *in vitro* for binding affinity, internalization, and cytotoxicity. The *in vivo* therapeutic efficacy of 5D3-DM1 ADC was evaluated in PSMA(+) PC3-PIP and PSMA(−) PC3-Flu mouse models of human PC. This therapeutic study has revealed that this new anti-PSMA ADC can successfully control the growth of PSMA(+) tumors without inducing systemic toxicity.

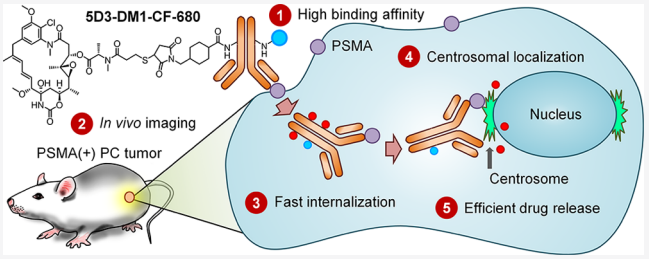

KEYWORDS: *prostate cancer, prostate-specific membrane antigen (PSMA), drug delivery, targeted therapy, antibody-drug conjugates (ADC), MCC linker, anti-PSMA antibody, 5D3 antibody, mertansine (DM1)*

1. INTRODUCTION

In the USA, prostate cancer (PC) is the most common cancer in men and the second leading cause of cancer-related death after lung and bronchus cancer. Over 174,000 American men were diagnosed with PC last year, and 18% of PC patients die yearly from this devastating decease.[1,2] Androgen deprivation therapy is initially effective in most metastatic PCs, but PCs eventually become resistant to hormone-based therapeutics and progress into castrate-resistant prostate cancer (CRPC).[3,4] At this stage, CRPC has typically metastasized to the bone and eventually to other vital organs of the body.[5] Second-line chemotherapeutics and hormone ablation therapies, such as docetaxel and enzalutamide and abiraterone, can extend survival; however, approximately 15−25% of patients will not respond to second-line therapy.[6,7] Novel targeted therapeutics are urgently needed to improve metastatic CRPC treatment by enhancing therapeutic efficacy and minimizing systemic toxicity.

Prostate-specific membrane antigen (PSMA) is an integral membrane protein with a molecular weight of 110 kDa and consisting of 750 amino acids.[8] PSMA is overexpressed in practically all malignant PC tumors compared to non-prostatic tissues.[9,10] It is also known that cancer aggressiveness, androgen blockage, and deprivation enhance PSMA expression levels.[11,12] Following binding by bioligands, such as anti-PSMA monoclonal antibodies (mAbs), low-molecular weight com-

Received: April 27, 2020
Revised: August 5, 2020
Accepted: August 6, 2020
Published: August 17, 2020

https://dx.doi.org/10.1021/acs.molpharmaceut.0c00457
Mol. Pharmaceutics 2020, 17, 3392−3402

pounds, and peptides, PSMA is readily internalized.[13,14] These characteristics make PSMA a perfect target for the development of diagnostic imaging probes and targeted therapeutics for PC.[15−18]

7E11 was the first anti-PSMA antibody originally developed using LNCaP PC cells as an antigen. The 7E11 mAb binds to the intracellular epitope of PSMA that is only exposed in apoptotic or necrotic PC cells.[19−21] Therefore, 7E11 mAb can be used as a bioligand for imaging PC but not for targeted therapy. Following the development of 7E11, a series of anti-PSMA mAbs were developed that targeted the extracellular moiety of PSMA. Some of anti-PSMA mAbs have been humanized, making them feasible for diagnosis or therapy without inducing the anti-mouse immune response. Among them, the humanized J591 mAb (HuJ591) was the most successful mAb, to date, with high binding affinity to the extracellular moiety of PSMA, and is widely used for PC imaging and radiotherapy. Following PSMA binding, the J591-PSMA complex internalizes quickly and localizes to endosomes in the cells, which enables efficient delivery of chemotherapeutics to the target cell. MLN2704 is an antibody-drug conjugate (ADC) that utilizes the anti-PSMA characteristics of HuJ591 for the targeted drug delivery of the anti-tubulin agent, mertansine (DM1), in PC therapy. However, MLN2704 has a narrow therapeutic window in metastatic CRPC therapy because of the poor stability of the disulfide linker.[22]

5D3 is a mAb that specifically binds to the extracellular domain of PSMA with sub-nanomolar affinity. This mAb has been previously used for targeted-imaging of PSMA(+) PCs.[23] By comparison, the binding affinities of 5D3 and J591 mAbs to PSMA are 0.14 and 1.2 nM, respectively, as determined by enzyme-linked immunosorbent assay. 5D3 mAb exhibits improved characteristics as a bioligand for targeting PC because of a nearly 10-fold higher binding affinity compared to J591.[24]

We have recently used 5D3 mAb for pretargeting therapy in PSMA(+) PC cells by the sequential treatment of 5D3-based pretargeting components, followed by a drug delivery component, which recognizes two components on the targeted cell surface by *trans*-cyclooctene-tetrazine bioorthogonal click chemistry.[25] Our proof-of-concept study revealed interesting results *in vitro*, showing a significant reduction of cell viability in PSMA(+) PC3-PIP PC cells compared to PSMA(−) PC3-Flu cells.[25] However, in animal models, an 8−24 h period is required to clear the unbound mAb from circulation before the second drug delivery component can be administered. Our *in vitro* studies revealed that 75% of surface-bound 5D3 mAbs are internalized within the first 2 h and remained inside cells for more than 24 h.[25] Within this time-frame, surface-bound 5D3 mAbs are internalized and not available on the cell surface. High binding affinity, fast internalization, and prolonged persistence of 5D3 in the cytoplasm are ideal factors for the development 5D3-based anti-PSMA ADCs for the therapy of PSMA(+) PC.

Our studies have also revealed that 5D3 mAb has a unique pattern of internalization in the target PC cells and it localizes to the centrosomal compartment in the vicinity of the nucleus. The centrosome is a cytoplasmic organelle, which serves as an organizing center for microtubule growth during the interphase of mitosis. Therefore, the 5D3 mAb can be conjugated with anti-tubulin drugs, such as mertansine (DM1) and paclitaxel, to directly deliver these agents to the centrosome and induce mitotic arrest and killing of cancer cells. Hence, our target-specificity is not limited to targeting PSMA(+) receptors on PC cells but also applies to specific delivery of drugs to the centrosome that is vital for cell division.

DM1 is used as a chemotherapeutic for ADC development and was discovered in the *Maytenus ovatus* shrub.[26−28] It is an anti-tubulin agent that inhibits the assembly of microtubules leading to the induction of mitotic arrest and the killing of cells at sub-nanomolar concentrations.[29] The antimitotic effects of maytansine derivatives are linked to their ability to bind to tubulin, inhibiting microtubule assembly.[30] DM1 is not target-specific and can attack healthy tissues as well, resulting in severe side effects and systemic toxicity.[31] To circumvent the lack of specificity, DM1 is typically conjugated to a target-specific antibody to be used as an ADC. The drug thiol functional group can be used for standard conjugation with antibodies without a reduction in toxicity. The unique characteristics of anti-PSMA 5D3 mAb: high target-specificity, enhanced binding affinity, fast internalization, and localization at the centrosome combined with the high cytotoxicity of DM1 can provide significant advantages for the development of the anti-PSMA 5D3-DM1-based ADC that targets PSMA(+) PC cells by mitotic arrest, leading to cell death.

2. MATERIALS AND METHODS

2.1. Antibody, Chemicals, and Reagents. Anti-PSMA mAb, 5D3 was produced following the protocol described previously and stored in 0.02% NaN_3/phosphate-buffered saline (PBS).[24] The drug, DM1, was purchased from Abcam, Inc. The heterobifunctional linker, sulfosuccinimidyl 4-(*N*-maleimidomethyl)cyclohexane-1-carboxylate (Sulfo-SMCC), amine-reactive fluorophores, Dulbecco's phosphate-buffered saline (DPBS), and BupH phosphate-buffered-saline were purchased from Thermo Fisher, Inc., and rhodamine B isothiocyanate−dextran (70 kDa) was purchased from Sigma-Aldrich, Inc. All organic solvents were of HPLC-grade, purchased from Fisher Scientific, and used without further purification.

2.2. Synthesis of ADC. The 5D3 mAb was buffer-exchanged from 0.02% NaN_3/PBS into 2 mM ethylenediaminetetraacetate (EDTA)/BupH PBS (pH 7.2) by 30 kDa MWCO ultracentrifugation filtration. A fraction of the 5D3 sample (5 mg in 1.0 mL of 2 mM EDTA/BupH PBS) was treated with freshly prepared Sulfo-SMCC [10-fold molar excess, 0.15 mg in 10 μL of anhydrous dimethyl sulfoxide (DMSO)] and stirred at ambient temperature for 2 h. The resulting product, 5D3-MCC (2.5 mg in 1.0 mL of 2 mM EDTA/BupH PBS), was treated with a 2-fold molar excess of DM1 (0.15 mg in 10 μL of anhydrous DMSO) over the linker. The mixture was stirred at ambient temperature for 24 h. For optical imaging, unconjugated 5D3 mAb or 5D3-MCC were labeled with fluorophores using 10 molar equivalents of amine-reactive fluorophores, AlexaFluor-488-NHS or CF-680-NHS, for 1 h at room temperature.

2.3. Ultracentrifugation and MALDI-TOF Analysis. Amicon ultracentrifugation filter units (4 or 15 mL capacity, 30 kDa MWCO) were used to exchange buffer, concentrate samples, and remove unreacted low-molecular weight reactants and byproducts after each step of the conjugation process. The samples were further purified by passing through Sephadex G-25 resin. ADCs and conjugates were also passed through a 0.22 μm membrane syringe filter for sterilization before drug administration. Molecular weights of intermediates and final products were determined using the Voyager DE-STR matrix-

https://dx.doi.org/10.1021/acs.molpharmaceut.0c00457
Mol. Pharmaceutics 2020, 17, 3392−3402

assisted laser desorption ionization time-of-flight (MALDI-TOF) mass spectrometer (Mass Spectrometry and Proteomics Facility, JHU School of Medicine). The average number of MCC heterobifunctional groups and DM1 molecules conjugated per mAb were 6 and 2.8, respectively, and were calculated based on the change in the molecular weight. The number of fluorophores conjugated per mAb was determined following the Thermo Fisher protocol for determination of the degree of labeling for amine-reactive probes. The size of ADC was measured by dynamic light scattering (DLS) using a Nano-ZS90 Zetasizer (Malvern Instruments, UK).

2.4. Cells. PSMA(+) PC3-PIP and PSMA(−) PC3-Flu cells were used to study the binding affinity, internalization, and therapeutic efficacy *in vitro* and to generate dual-tumor mouse models. Both cell types were grown in RPMI 1640 medium (supplemented with 10% FBS and 1% penicillin−streptomycin) and maintained in a humidified incubator at 37 °C in a 5% CO_2 atmosphere. Cells were confirmed to be free of mycoplasma contamination.

2.5. Cell Analysis by Flow Cytometry. 5D3-DM1 ADC binding affinity was tested in PC3-PIP and PC3-Flu cells seeded in a 6-well plate (0.4 million/well) and grown for 24 h to ∼60% confluency. Fluorescent 5D3-DM1-AF-488 or 5D3-AF-488 (20 μg/mL) was incubated with cells for 30 min at 4 °C. Unbound excess mAbs or ADCs were washed once using DPBS, and cells were harvested by trypsinization. Cells were resuspended in buffer and fixed by 4% paraformaldehyde (PFA). Cells were analyzed on a BD LSR II flow cytometer using 488 nm laser for AlexaFluor 488. Fluorescence histograms for DM1 conjugated and unconjugated 5D3 on PSMA(±) cells were generated by FlowJo software.

2.6. *In Vitro* Optical Imaging. Internalization and localization of 5D3 mAb and its drug conjugates were studied in PSMA(±) cells. PSMA(+) PC3-PIP or PSMA(−) PC3-Flu cells were seeded (4-well chamber slides, 0.2 million cells per well) and grown for 1−2 days to 80−90% confluency. Medium was removed in each chamber, and cells were treated with 150 μL of 20 μg/mL of 5D3-AF-488 or 5D3-DM1-AF-488 and incubated at 37 °C for 30 min, 1, 6, 12, and 24 h under 5% CO_2 in a humidity-controlled incubator. For one chamber treated with 5D3-AF-488, cells were pulsed with 70 kDa rhodamine−dextran (100 μg/mL) along with 5D3-AF-488. Cells were washed with DPBS for 5 min and fixed by 4% PFA on ice for 10 min. Nuclei were counterstained using Hoechst 33342 (10 μg/mL in H_2O at RT for 10 min) and wet-mounted. The images were collected using a Zeiss Axiovert 200 fluorescence microscope system equipped with an LSM 510-Meta confocal module and processed using Zeiss Zen software.

2.7. Cytotoxicity of 5D3-DM1 in PSMA(±) Cells. Cytotoxicity and cell viability were assayed by treating PC3-PIP and PC3-Flu cells in 96-well plates in RPMI 1640 culture media with 5D3-DM1 ADC over a range of concentrations. Briefly, cells were seeded in a 96-well plate (2000 cells/well) and grown for 24 h to 40−50% confluency. Wells were treated with increasing concentrations of 5D3-DM1 or pure DM1 equivalent to the DM1 concentration in 5D3-DM1 ADC (1; 10; 100; 1000; 10,000; and 100,000 ng/mL). After 48 h incubation, IC_{50} values of 5D3-DM1 ADC and corresponding free DM1 were determined using the WST-8 assay (Dojindo Molecular Technologies), following the manufacturer's protocol. Briefly, cells in each well in 100 μL of the fresh media were treated with 10 μL of WST-8 reagent and incubated at 37 °C. During incubation, WST-8 tetrazolium salt is reduced by dehydrogenase in living cells, forming a yellow formazan dye with λ_{max} at 450 nm. After 3 h, the absorbance was measured at 450 nm. The concentration of the formazan dye in the media produced by dehydrogenases is directly proportional to the density of viable cells in the well. The cell viability of treated cells was normalized to readings in untreated control cells, which were considered to have 100% viability. Data were fitted, and IC_{50} values for DM1 and 5D3-DM1 were calculated using Prism (GraphPad, San Diego CA).

2.8. Human PC Animal Models. Healthy, four-to-six-week-old, male athymic nude mice were used for this study. For PSMA(+) and PSMA(−) dual-tumor mouse models, PC3-PIP and PC3-Flu cells were grown to 70−80% confluency in RPMI 1640 media, trypsinized, and 5×10^6 cells were reconstituted in 50 μL of RPMI 1640/Matrigel (1:1) for each inoculation and maintained at 4 °C. PSMA(±) cells were subcutaneously inoculated in the left and right flanks of the animal. When each tumor volume reached 100−150 mm^3 in size, mice were used for *in vivo* imaging and therapeutic and toxicological studies. All animal experiments were carried out in accordance with protocols approved by the Johns Hopkins University Animal Care and Use Committee and were conducted in strict compliance with all federal and institutional guidelines. At the end of imaging and therapeutic experiments, mice were euthanized according to the protocol.

2.9. Determination of *In Vivo* Therapeutic Efficacy. Four groups of male athymic nude mice, subcutaneously inoculated with PC3-PIP and PC3-Flu human PC cells, were administered three different doses of 5D3-DM1-CF-680 (1.0, 2.5, and 5.0 mg/kg in 200 μL of saline) and 200 μL of saline for the control group. Mice were imaged using a Xenogen IVIS 200 Optical Imaging system to confirm the tumor uptake of 5D3-DM1-CF-680. The second therapeutic dose was given after two weeks. The sizes of the tumors were measured with a caliper every other day during the complete treatment. The tumor volume was calculated using the formula $(L \times W^2)\pi/6$, where L is the longest diameter (the major axis) and W is the tumor width, measured perpendicular to the major axis.

2.10. Toxicological Study. The live toxicological assessment included daily clinical observations, body weight measurements every other day, and food consumption. After the 3-week treatment, animals were euthanized and the blood was immediately collected for complete blood count (CBC) and for the analysis of the toxicological chemistry profile. Blood urea nitrogen (BUN), alanine aminotransferase (ALT), and aspartate aminotransferase (AST) were analyzed to determine the long-term liver and kidney toxicity of the drug. After euthanization, tumors and vital organs, liver, kidney, heart, spleen, lungs, sternum, small intestine, colon, and gallbladder, were extracted, preserved in 10% neutral-buffered formalin, and embedded in paraffin. H&E staining was performed on 4 μm sections following a standard protocol. Toxicology studies were carried out in treated and untreated tumor-bearing mice and healthy mice. Metastatic tumors in vital organs were also preserved for future analyses.

2.11. Statistical Analysis. The *in vitro* therapeutic study was executed in triplicate per plate, and duplicate independent experiments were conducted for statistics. The one-way analysis of variance (ANOVA) was used for the omnibus F-test. Changes in the cell viability were considered significant (p value < 0.05) when the F value was greater than the critical value of the F-distribution. In *in vivo* experiments, the statistical

https://dx.doi.org/10.1021/acs.molpharmaceut.0c00457
Mol. Pharmaceutics 2020, 17, 3392−3402

Scheme 1. Synthesis of the 5D3-DM1 ADC and Its Fluorescence Analogues[a]

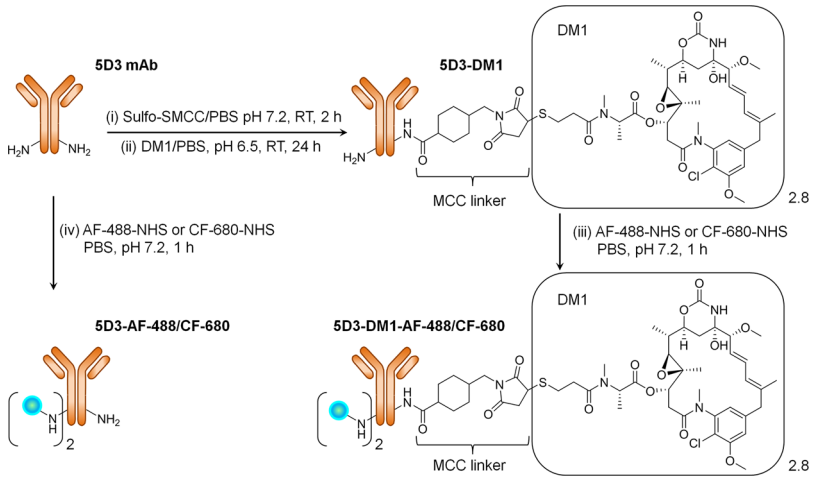

[a]In the first step, 5D3 mAb was functionalized by reaction with the Sulfo-SMCC heterobifunctional linker (i) and conjugated with DM1 (ii). The resulting 5D3-DM1 (iii) and 5D3 mAbs (iv) were labeled with AF-488 (for *in vitro* imaging and flow cytometric analysis) or CF-680 (for *in vivo* optical imaging).

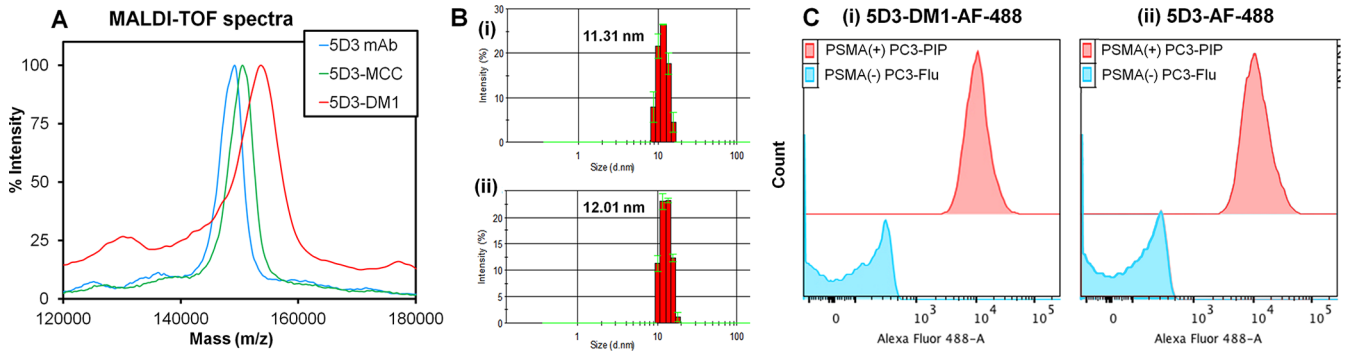

Figure 1. Characterization of 5D3-DM1 ADC. (A) MALDI-TOF spectra of 5D3 mAb, intermediate 5D3-MCC, and 5D3-DM1 ADC. (B) DLS analysis and size distribution of 5D3 mAb (i) and 5D3-DM1 (ii). (C) Fused flow cytometric histogram of PSMA(+) PC3-PIP and PSMA(−) PC3-Flu cells labeled with 5D3-DM1-AF-488 (i) and 5D3-AF-488 (ii), showing that there is no change in the PSMA labeling properties of 5D3 after modification. Note: Histograms were plotted in red (PC3-PIP cells) and blue (PC3-Flu cells) for both 5D3-DM1-AF-488 and 5D3-AF-488 for direct comparison.

analysis (*t*-test) between multiple-dose treated and untreated groups was performed using JMP 12.1.0 Statistical Discovery from SAS. A p value of less than 0.05 was considered significant ($*p < 0.05$). Survival curves in Kaplan−Meier analysis use the time when the tumor has reached a four-fold increase in the volume relative to the initial tumor volume as the surrogate endpoint.

3. RESULTS

3.1. Synthesis of 5D3-DM1 ADCs. In the synthesis of 5D3-DM1 ADC, approximately six MCC groups were conjugated per antibody molecule (Scheme 1). Two equivalents of DM1, with respect to the number of attached MCC groups, were used for the drug conjugation. The final ADC had an average of 2.8 DM1 molecules per antibody. Because DM1 is a hydrophobic molecule, a 24 h reaction time in the rotating mixer was required for this conjugation. The resulting ADC was labeled with AlexaFluor 488 or CF-680 NIR fluorophores for *in vitro* imaging and flow cytometry or *in vivo* imaging experiments, respectively. Unconjugated 5D3 mAb was also labeled with AF-488 dyes for control imaging and flow cytometry. The average number of fluorophores per antibody was maintained as approximately two. The molecular weights of 5D3-MCC and 5D3-DM1 ADC were measured by MALDI-TOF. The number of conjugated groups and drugs was determined based on the shift of molecular weights, as shown in Figure 1A. Changes in size after modifications determined by DLS were not statistically significant (Figure 1B).

3.2. Cell Analysis by Flow Cytometry. Figure 1C shows the histograms of PC3-PIP and PC3-Flu cells treated with 5D3-DM1-AF-488 or 5D3-AF-488. PC3-PIP cells overexpress PSMA compared to PC3-Flu cells. There were no significant changes between the histograms of cells treated with 5D3-DM1-AF-488 and 5D3-AF-488, proving that the conjugation of drug molecules does not change the PSMA-specificity and binding properties of 5D3 mAb.

3.3. *In Vitro* Cellular Imaging. PSMA(+) PC3-PIP cells were labeled with fluorescent 5D3-AF-488 and 5D3-DM1-AF-488 conjugates, and confocal images are shown in Figure 2. Both mAb and ADC were internalized quickly and localized in the cytoplasm within 30 min and remained in the cell for more than 24 h. Unlike other cancer-cell-specific antibodies (Figure S1), both 5D3 (Figure 2A) and 5D3-DM1 ADC (Figure 2B)

https://dx.doi.org/10.1021/acs.molpharmaceut.0c00457
Mol. Pharmaceutics 2020, 17, 3392−3402

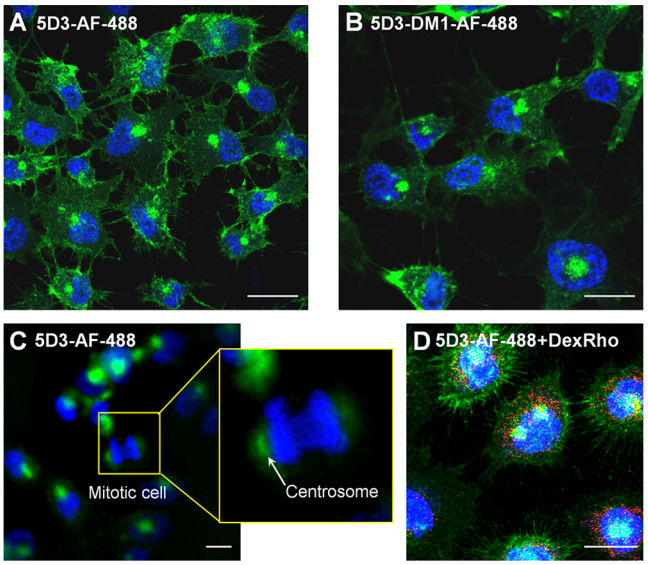

Figure 2. Confocal fluorescence images of 5D3 mAb and 5D3-DM1 ADC in PSMA(+) PC3-PIP cells. Internalized 5D3-AF-488 (A) and 5D3-DM1-AF-488 (B) after 1 h. (C) Perinuclear localization of 5D3-AF-488. (D) Cells treated with 5D3-AF-488 (green) and dextran–rhodamine (red, visualizing endosomes), a dividing cell exhibiting the mAbs localized to the centrosomes. (Scale bar: 50 μm).

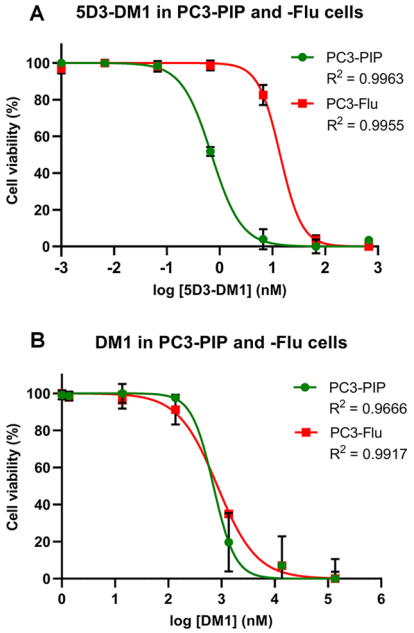

Figure 3. *In vitro* cytotoxicity in PC3-PIP and PC3-Flu cells. (A) Cytotoxicity of 5D3-DM1 in PSMA(+) PC3-PIP (IC_{50} = 0.70 nM) and PSMA(−) PC3-Flu (IC_{50} = 13.98 nM) cells. (B) Cytotoxicity of DM1 equivalent to 5D3-DM1 in PSMA(+) PC3-PIP (IC_{50} = 603.8 nM) and PSMA(−) PC3-Flu (IC_{50} = 735.2 nM) cells. IC_{50} values were calculated using the GraphPad/Prism software.

were localized in the vicinity of the nucleus immediately after internalization. This unique behavior was further analyzed by observing dividing cells at high resolution (Figure 2C). The enlarged view in Figure 2C shows a late anaphase stage of a mitotic cell. The 5D3-AF-488 conjugate appears to be associated with the centrosomes of dividing cells. When cells are incubated with 5D3-AF-488 and co-treated with the rhodamine-B dextran (70 kDa) endosome marker, the two-color images reveal that 5D3 localization does not overlap with late endosomes and lysosomes (Figure 2D). No significant uptake of 5D3-DM1 ADC was observed in PSMA(−) PC3-Flu cells (Figure S2).

3.4. *In Vitro* Therapeutic Study. The 5D3-DM1 ADC and unconjugated DM1 were used for microscale determination of the drug cytotoxicity in PSMA(+) PC3-PIP and PSMA(−) PC3-Flu cells (Figure 3). For the direct comparison of cytotoxicity, the dose was normalized for DM1 concentrations in nM. The most pronounced cytotoxicity was observed for PSMA(+) PC3-PIP cells treated with 5D3-DM1, with a corresponding IC_{50} value of 0.70 nM (Figure 3A). The same drug in PSMA(−) PC3-Flu cells had an IC_{50} of 13.98 nM. Cell treatment with matching concentrations of the free DM1 drug was less toxic for both PC3-PIP and PC3-Flu cells, with IC_{50} values of 603.8 and 735.2 nM, respectively (Figure 3B). These results suggest that the cytotoxicity of 5D3-DM1 was target-mediated by the antibody.

3.5. *In Vivo* Therapeutic Efficacy. PSMA(+) PC3-PIP and PSMA(−) PC3-Flu dual-tumor mouse models were used in this study following the treatment schedule shown in Figure 4A. In this study, we selected three doses for the treatment plan to evaluate the therapeutic efficacy of the drug. Four groups of mice were treated with increasing doses of 5D3-DM1 (1.0, 2.5, and 5.0 mg/kg, and saline as a control). The second dose was administered on day 14. On day 21, mice were euthanized and the toxicological profiles were evaluated in all mice. A day after the administration of the second dose of 5D3-DM1-CF-680, dual-tumor mice were imaged using a Xenogen IVIS 200 Optical Imaging system (Figure 4B). Compared to the untreated mice [Figure 4B(i)], 5D3-DM1-CF-680 treated mice showed a high tumor uptake by the PSMA(+) PC3-PIP tumor [Figure 4B(ii)]. The volumes of PC3-PIP tumors in 5D3-DM1-CF-680 treated mice were smaller than that of PSMA(−) or untreated tumors. Only a slight uptake of ADC was seen in the PC3-Flu tumor in the same mouse.

The therapeutic effects of 5D3-DM1-CF-680 in PSMA(+) PC3-PIP tumors are shown in Figure 5. In this study, mice treated with the highest dose of 5.0 mg/kg showed the maximum, and statistically significant, therapeutic efficacy in PSMA(+) tumors compared to all other doses; however, 5.0 mg/kg is not the maximum tolerated dose for 5D3-DM1-CF-680. As shown in Figure 5A, the relative tumor volume was significantly lower ($*p < 0.05$) from day 15 onward with respect to the untreated group. At the end of the therapy, the 2.5 mg/kg dose treatment also provided significantly higher therapeutic efficacy compared to the 1.0 mg/kg dose and saline treatment ($\#p < 0.05$) at day 21. However, the 1.0 mg/kg dose was unable to produce significant therapeutic efficacy. The treatment response of PSMA(−) PC3-Flu tumors was observed, and the results are shown in Figure 5B. Interestingly, the growth rate of PC3-Flu tumors was slightly lower compared to the untreated mice; however, it was not statistically significant at any dose regimen.

Figure 5C shows changes in relative tumor volumes among PSMA(+) PC3-PIP and PSMA(−) PC3-Flu tumors in multiple treatment groups on day 21 (end of the treatment). The overall efficacy was higher in PSMA(+) tumors and the 5.0 mg/kg dose group exhibited significantly ($*p < 0.05$) higher therapeutic efficacy in PSMA(+) tumors compared to PSMA(−) tumors. The 2.5 mg/kg treatment was not

https://dx.doi.org/10.1021/acs.molpharmaceut.0c00457
Mol. Pharmaceutics 2020, 17, 3392−3402

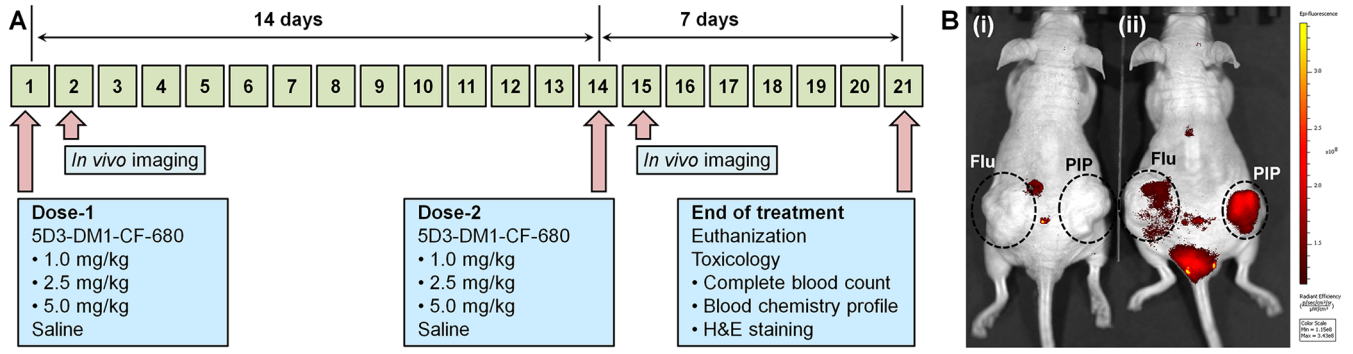

Figure 4. *In vivo* therapeutic study. (A) Dosing schedule of *in vivo* therapy, imaging, and toxicological study. (B) *In vivo* NIR fluorescence images of drug delivery. The tumor uptake of 5D3-DM1-CF-680 in PSMA(+) PC3-PIP and PSMA(−) PC3-Flu dual-tumor mouse models. (i) Untreated and (ii) treated with 2.5 mg/kg of 5D3-DM1-CF-680. Images were obtained 24 h after the administration of ADC at day 15.

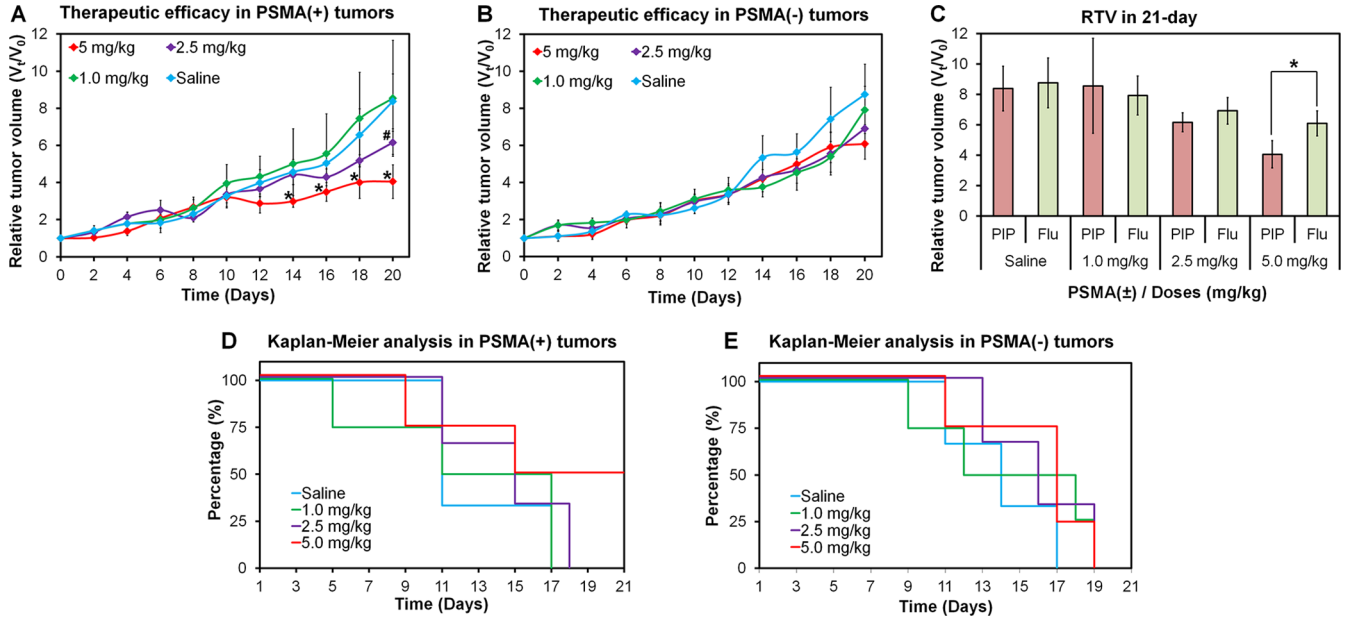

Figure 5. *In vivo* therapeutic effect of 5D3-DM1-CF-680 in human PC xenograft mouse models (n = 6/group). Therapeutic efficacy of 5D3-DM1-CF-680 (1.0, 2.5, and 5.0 mg/kg) in (A) PSMA(+) PC3-PIP PC tumors and (B) PSMA(−) PC3-Flu PC tumors in mouse models. (C) Relative tumor volumes at day 21 in mice treated with multiple-doses for PC3-PIP and PC3-Flu tumors. The Kaplan−Meier analysis of the surrogate survival. Kaplan−Meier graphs were plotted using the time taken to reach four times the initial tumor size as the endpoint in (D) PSMA(+) PC3-PIP PC tumors and (E) PSMA(−) PC3-Flu PC tumors in mouse models (n = 10/group).

significantly efficacious when PSMA(+) and PSMA(−) tumors were compared. Overall, the 5.0 mg/kg dose showed a statistically significant therapeutic efficacy in PSMA(+) tumor models compared to all other dose treatment groups, the untreated group, and PSMA(−) tumors.

The Kaplan−Meier surrogate survival results for untreated mice and mice treated with 5D3-DM1-CF-680 are shown in Figure 5D,E. The results demonstrated that the 5.0 mg/kg treatment increased the survival of mice with PSMA(+) tumors (*p < 0.05), and approximately, 50% of tumors did not reach the four-fold relative tumor size during the treatment. All other treated and untreated PSMA(+) and PSMA(−) tumors exceeded four-fold relative tumor growth before day 19.

3.6. Systemic Toxicity of the Therapy. At day 21, mice were euthanized and blood was collected for CBC and toxicology chemical profile analyses. The CBC showed no significant change between healthy, tumor-bearing untreated, and treated mice. BUN (Figure 6A) and ALT (Figure 6B) levels in treated and untreated mice were within the normal range; however, AST (Figure 6C) was elevated in both the untreated and treated tumor-bearing groups. Mice were weighed every other day to evaluate the *in vivo* toxicity of 5D3-DM1 (Figure 6D). A slight weight loss was observed in all treated mice; however, it was insignificant compared to untreated healthy mice. The H&E staining was performed in fixed tissue samples and did not show organ toxicity of the treatment in any of the experimental mice. Figure 7 shows high necrosis in PSMA(+) PC3-PIP tumors (Figure 7A) compared to PSMA(−) PC3-Flu tumors (Figure 7B), the animal group treated with the 5.0 mg/kg dose. However, we observed necrosis in both tumor models that is typically observed in large experimental tumors. We observed no tissue damage in the liver and kidney of mice treated with the 5.0 mg/kg dose (Figure 7C).

4. DISCUSSION

PSMA is widely used as a biomarker to image PC, drug delivery, and radioligand therapy.[32−35] PSMA-specific small

https://dx.doi.org/10.1021/acs.molpharmaceut.0c00457
Mol. Pharmaceutics 2020, 17, 3392−3402

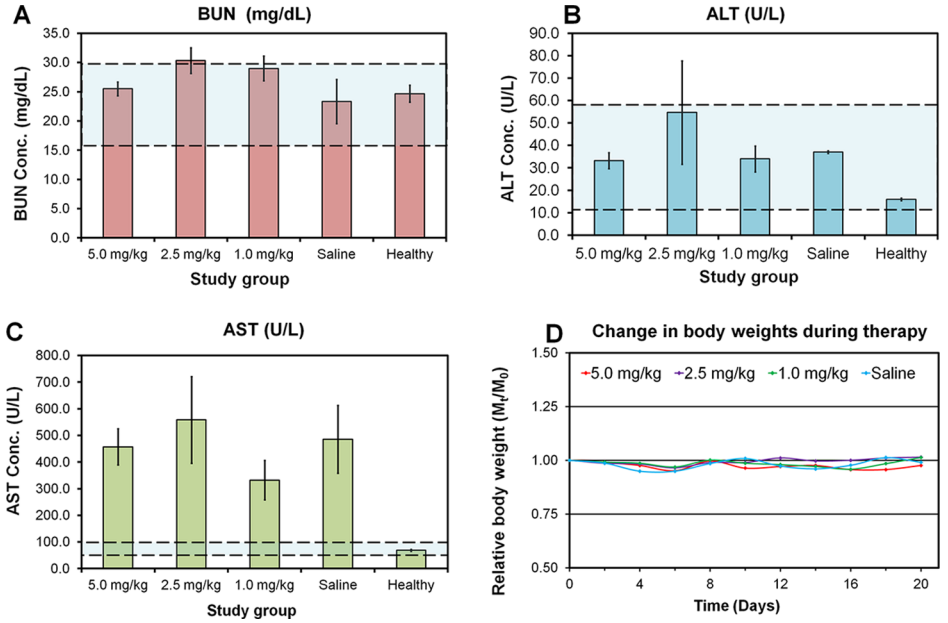

Figure 6. Toxicological study of 5D3-DM1-CF-680 ADC therapy (n = 4/group). (A) BUN (healthy range 16−30 mg/dL), (B) ALT (healthy range 15−60 U/L), (C) AST (healthy range 50−100 U/L) concentrations for ADC-treated and saline-treated in PSMA(+) PC3-PIP and PSMA(−) PC3-Flu dual-tumor mouse models, and (D) changes in the animal body weight during the therapy relative to the initial body weight (n = 6/group).

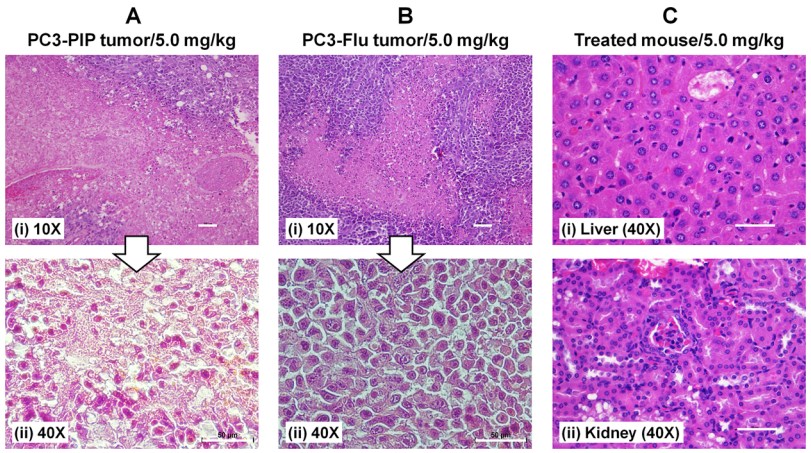

Figure 7. H&E staining of tumors and organs in a 5.0 mg/kg dose-treated mouse. (A) PSMA(+) tumor at 10× (i) and 40× (ii). (B) PSMA(−) tumor at 10× (i) and 40× (ii). (C) Liver tissue (i) and kidney tissue (ii) at 40×. Study shows high necrosis in the PSMA(+) PC3-PIP tumor, low necrosis in the PSMA(−) PC3-Flu tumor, and no toxicological damage in the liver or kidney. (Scale bars: 100 μm in 10× images and 50 μm in 40× images).

molecules, peptides, and mAbs are used as the bioligands with which to target PSMA. The 5D3 antibody has a sub-nanomolar affinity for PSMA, and we have previously used this antibody for pretargeting therapy and proved the concept *in vitro*. The *in vivo* pretargeting therapy with 5D3 mAb is challenging because of its fast internalization rates. Nevertheless, high target-specificity and affinity, together with the fast internalization rate, make 5D3 mAb an ideal bioligand with which to target PSMA and serve as a platform for the development of therapeutics. In addition, after internalization, 5D3 localizes to the centrosome, an organelle critical for cell division. The centrosome organizes microtubules during cell division; hence, 5D3 is ideal for delivering anti-tubulin agents to this organelle. We are currently studying the specific mechanisms that drive 5D3 localization to centrosomes and suggest that a receptor-mediated specificity is involved in this phenomenon.

The anti-tubulin agent, DM1, has been successfully used for the development of ADC to treat other cancers. For example, trastuzumab- and DM1-based T-DM1, developed through amine conjugation chemistry, is a novel FDA-approved ADC used to treat HER2(+) breast cancer (IC_{50} = 0.22−4.26 nM).[36] PSMA-targeting small therapeutic molecules have also been tested to treat PSMA(+) PC, and most of them have an IC_{50} in the nanomolar range (1−800 nM).[37] Nevertheless, DM1 is still a popular drug in ADC development.[29] In T-DM1, the anti-HER2 trastuzumab is conjugated with DM1 through an MCC linker. We used the same MCC conjugation chemistry in 5D3-DM1 development, rather than a disulfide linkage to avoid the rapid dissociation as seen with the MLN2704.[22] There was no significant degradation of 5D3-DM1 observed in PBS storing for 9 months at 4 °C (Figure

https://dx.doi.org/10.1021/acs.molpharmaceut.0c00457
Mol. Pharmaceutics 2020, 17, 3392−3402

S3). The complete stability test for 5D3-DM1 in PBS and plasma will be performed in the future.

In 5D3-DM1 ADC synthesis, 5D3 mAb was first functionalized with maleimide groups by conjugation with an MCC linker using amine-NHS ester conjugation chemistry. Amino groups are common in proteins, and this conjugation chemistry is widely used for mAb modification with drugs and imaging agents. Non-specificity and lack of control in the reaction are challenges in amine conjugation of mAbs. Amine conjugation also has limited control in maintaining the reproducibility of the drug loading. We judiciously maintained the reaction conditions, such as molar equivalent, concentration of reactants, pH, agitation, and temperature, to ensure the consistency of drug loading. The number of MCC groups per mAb was limited to six. After purification, two equivalents of DM1, with respect to the total molar content of MCC groups in the reaction, were reacted with 5D3-MCC. Precise control and maintenance of the MCC load and equivalents of the reactants are important so that the mAb is not overloaded with hydrophobic DM1 that could lead to mAb precipitation. Batches of unconjugated 5D3 and 5D3-DM1 ADCs were labeled with suitable fluorophores for direct *in vitro* and *in vivo* optical imaging. Therefore, the mAb and its conjugates could be tracked without the use of secondary antibodies.

The molecular weights of 5D3-MCC and 5D3-DM1 were measured by MALDI-TOF. The number of conjugated moieties per mAb was calculated based on the shifts in molecular weights. We performed flow cytometry analysis to observe any adverse changes in 5D3 for PSMA upon conjugation. Flow cytometry results revealed that there was no change in the PSMA labeling properties of 5D3 after modification. In this study, the total conjugation in fluorescent 5D3-DM1 was maintained at no more than 12 groups per antibody. For comparison, we and others have previously observed that up to 20 foreign groups can be substituted per trastuzumab without altering its binding affinity.[38−40]

Unlike other antibodies, which follow receptor-mediated clathrin endocytosis, 5D3 mAb almost immediately localizes to the vicinity of the nucleus (Figure 2C). The same phenomenon was observed after 5D3 was conjugated with DM1 to form 5D3-DM1 ADCs. High-resolution confocal images of mitotic cells revealed that 5D3 mAb localizes to the centrosome. We postulate that specific delivery of anti-tubulin agents to the centrosomes is a crucial factor for the success of 5D3 ADC therapy. Images of PC3-PIP cells treated with 5D3-AF-488 and rhodamine-labeled dextran to distinguish the centrosome and endosome compartments revealed that these compounds are localized in different cellular compartments and that internalized 5D3 mAbs are likely localized at the centrosomes. The specific mechanisms of this phenomenon are still unresolved and are the subject of our ongoing research.

In vitro assays showed that the PSMA(+) PC3-PIP cell line is highly sensitive to treatment with the 5D3-DM1 that demonstrated the lowest IC_{50} value of 0.70 nM compared to PCMA(−) PC3-Flu cells (IC_{50} = 13.98 nM). Interestingly, the control study, using free DM1 with a dose equal to the drug content in ADC, exhibited IC_{50} values of 603.8 and 735.2 nM for PC3-PIP and PC3-Flu cells, respectively. The preclinical IC_{50} value for MLN2704 is 1.4 nM for PSMA(+) LNCaP cells compared to 61.3 nM for PSMA(−) PC3 cells.[41] Successful results of *in vitro* studies highlighted the potential and provided the rationale to use 5D3-DM1 ADCs *in vivo* to determine the therapeutic efficacy and toxicological effects in preclinical models of PSMA(+) human PC.

We have shown that 5D3-DM1-CF-680 is effective in *in vivo* subcutaneous dual xenograft mouse models of human PC. Two doses of 2.5 and 5.0 mg/kg 5D3-DM1 ADC resulted in a significant reduction of PSMA(+) PC3-PIP tumors compared to PSMA(−) PC3-Flu tumors. However, the 1.0 mg/kg dose was not sufficient to impair tumor growth. We also observed an insignificant reduction of PSMA(−) tumors compared to untreated mice, presumably because of nonspecific accumulation and degradation of cytotoxic ADCs in the tumor due to the enhanced permeability and retention (EPR) effect.[42,43] The highest dose used in the study, 5.0 mg/kg, was below the maximum tolerated dose. However, we suggest that the high therapeutic efficacy of 5D3-DM1 in PSMA(+) tumors is attributable to the combination of efficient delivery of ADC to the tumor by the EPR effect, specific targeting of the PSMA(+) cancer cell surface receptor, and rapid internalization and intracellular delivery of the cytotoxic cargo to the centrosome within the target cancer cell. The results of the study demonstrate a significant effect of the 5D3-DM1 targeted therapy in PC3-PIP tumors treated with the 5.0 mg/kg dose compared to the low-dose treatments ($*p < 0.05$). Fifty percent of PSMA(+) PC animals survived without reaching the surrogate survival endpoint (four times the initial tumor volume) during the 21 day treatment with 5.0 mg/kg 5D3-DM1. In all other groups treated with lower doses, including PSMA(−) models, tumors reached four times the initial tumor volume limit before the therapy was completed.

No clinical manifestations of systemic toxicity were detected in mice treated with 5D3-DM1. During the course of the treatment, the mean body weight of mice in each treatment group remained practically unchanged, including healthy mice and mice treated with 5D3-DM1 (Figure 6D). The platelet (PLT) count dropped, and the white blood cell (WBC) count was elevated after treatment; however, all counts were still within the healthy range (Figure S4).

We observed no pathological alterations in liver, kidney, heart, spleen, lungs, sternum, small intestine, colon, or gallbladder in treated animals. Metastatic tumors were observed in the kidneys of untreated mice (Figure S5) but not in treated mice. Considerably large necrotic areas were seen in both treated and untreated PSMA(+) and PSMA(−) (Figure 7). The inner regions of solid tumors received insufficient blood supply, resulting in oxygen and glucose deprivation and necrosis.[44−47] Hence, we believe that extensive necrosis in the core of untreated and PSMA(−) tumors is due to these ischemic conditions.

5. CONCLUSIONS

We have developed a novel ADC for the treatment of PC using the high target-specificity, binding affinity, and centrosomal localization of anti-PSMA 5D3 mAb and high cytotoxicity of DM1. The 5D3-DM1 ADC labeled with imaging agents demonstrated a high and homogeneous tumor uptake in PSMA(+) tumors. The 5D3-DM1 conjugates also resulted in a high tumor response without any notable adverse systemic effects. Antibody modification using amine functional groups did not alter its binding with PSMA. Two cycles of treatment using a 5.0 mg/kg dose provided efficient control of PSMA(+) tumor growth, which resulted in 50% of mice surpassing the 21 day duration of the study. The treatment was also safe, as, in our studies, we observed no clinical manifestations, weight loss,

https://dx.doi.org/10.1021/acs.molpharmaceut.0c00457
Mol. Pharmaceutics 2020, 17, 3392−3402

or adverse changes in the CBC and blood chemistry of the treatment groups, except for the elevation of the AST level and the reduction of the PLT count due to complications of large tumors. The H&E of vital organs, including the liver and kidney, did not show any necrosis or tissue damage. Almost all tumors have a necrotic core induced by oxygen and glucose deprivation at the end of treatment. Based on our experimental results, we are confident that 5D3-DM1 can become a new and highly efficacious therapy for aggressive PC. We envision future clinical applications of this strategy, which will increase the therapeutic efficacy while minimizing the systemic toxicity in PC patients possibly before metastasis into vital organs and bones.

■ ASSOCIATED CONTENT

Supporting Information

The Supporting Information is available free of charge at https://pubs.acs.org/doi/10.1021/acs.molpharmaceut.0c00457.

Fluorescence images of 5D3, anti-AXL, and trastuzumab mAbs in PC3-PIP, MDA-MB-231, and BT-474 cancer cells; PC3-Flu cells treated with 5D3-DM1; MALDI-TOF spectra showing the stability of 5D3-DM1; graphs of PLT and WBC levels in treated and untreated mice; and an image of metastatic tumors found on the kidneys of an untreated mouse (PDF)

■ AUTHOR INFORMATION

Corresponding Author

Sudath Hapuarachchige − *The Russell H. Morgan Department of Radiology and Radiological Science, The Johns Hopkins University School of Medicine, Baltimore, Maryland 21205, United States;* orcid.org/0000-0002-1166-8247; Phone: +1(443) 287-4426; Email: shapuar1@jh.edu; Fax: +1(410) 614-1948

Authors

Colin T. Huang − *The Russell H. Morgan Department of Radiology and Radiological Science, The Johns Hopkins University School of Medicine, Baltimore, Maryland 21205, United States*

Xin Guo − *Department of Molecular and Comparative Pathobiology, The Johns Hopkins University School of Medicine, Baltimore, Maryland 21205, United States*

Cyril Bařinka − *Laboratory of Structural Biology, Institute of Biotechnology of the Czech Academy of Sciences, BIOCEV, 252 50 Vestec, Czech Republic;* orcid.org/0000-0003-2751-3060

Shawn E. Lupold − *The James Buchanan Brady Urologic Institute and Department of Urology, Johns Hopkins School of Medicine, Baltimore, Maryland 21287, United States*

Martin G. Pomper − *The Russell H. Morgan Department of Radiology and Radiological Science and Department of Oncology, the Sidney Kimmel Comprehensive Cancer Center, The Johns Hopkins University School of Medicine, Baltimore, Maryland 21205, United States; The James Buchanan Brady Urologic Institute and Department of Urology, Johns Hopkins School of Medicine, Baltimore, Maryland 21287, United States;* orcid.org/0000-0001-6753-3010

Kathleen Gabrielson − *Department of Molecular and Comparative Pathobiology, The Johns Hopkins University School of Medicine, Baltimore, Maryland 21205, United States*

Venu Raman − *The Russell H. Morgan Department of Radiology and Radiological Science and Department of Oncology, the Sidney Kimmel Comprehensive Cancer Center, The Johns Hopkins University School of Medicine, Baltimore, Maryland 21205, United States*

Dmitri Artemov − *The Russell H. Morgan Department of Radiology and Radiological Science and Department of Oncology, the Sidney Kimmel Comprehensive Cancer Center, The Johns Hopkins University School of Medicine, Baltimore, Maryland 21205, United States*

Complete contact information is available at: https://pubs.acs.org/10.1021/acs.molpharmaceut.0c00457

Notes

The authors declare no competing financial interest.

■ ACKNOWLEDGMENTS

This study was mainly supported by the Emerson Collective Cancer Research Fund (2018 Emerson Collective 128821). This work was partially supported by the DOD (W81XWH-16-1-0595), the NIH/NCI R01CA209884, and the NIH/NIBIB (P41EB024495). This work was, in part, supported by the CAS (RVO: 86652036), CSF (18-04790S), and IOCEV/ERDF (CZ.1.05/1.1.00/02.0109). The authors acknowledge Dixie Hoyle and Zora Novakova for their assistance in flow cytometry and antibody purification, respectively.

■ ABBREVIATIONS

ADC, antibody-drug conjugate; DM1, mertansine; DPBS, Dulbecco's phosphate buffered saline; mAb, monoclonal antibody; MALDI-TOF, matrix-assisted laser desorption ionization time-of-flight mass spectrometry; PBS, BupH phosphate buffered saline; PC, prostate cancer; PSMA, prostate-specific membrane antigen; SEC, size-exclusion chromatography; Sulfo-SMCC, sulfosuccinimidyl 4-(*N*-maleimidomethyl)cyclohexane-1-carboxylate

■ REFERENCES

(1) Siegel, R. L.; Miller, K. D.; Jemal, A. Cancer Statistics, 2019. *Ca—Cancer J. Clin.* **2019**, *69*, 7−34.

(2) Siegel, R. L.; Miller, K. D.; Jemal, A. Cancer Statistics, 2020. *Ca—Cancer J. Clin.* **2020**, *70*, 7−30.

(3) Cho, S.; Zammarchi, F.; Williams, D. G.; Havenith, C. E. G.; Monks, N. R.; Tyrer, P.; D'Hooge, F.; Fleming, R.; Vashisht, K.; Dimasi, N.; et al. Antitumor Activity of Medi3726 (Adct-401), a Pyrrolobenzodiazepine Antibody-Drug Conjugate Targeting Psma, in Preclinical Models of Prostate Cancer. *Mol. Cancer Ther.* **2018**, *17*, 2176−2186.

(4) Semenas, J.; Allegrucci, C.; Boorjian, S.; Mongan, N.; Liao Persson, J. Overcoming Drug Resistance and Treating Advanced Prostate Cancer. *Curr. Drug Targets* **2012**, *13*, 1308−1323.

(5) Phillips, R. M.; Deek, M. P.; Deweese, T. L.; Tran, P. T. Metastasis-Directed Therapy in Prostate Cancer. Why, When, and How? *Oncology*, **2019**, *33*, 394−399.

(6) Antonarakis, E. S.; Lu, C.; Wang, H.; Luber, B.; Nakazawa, M.; Roeser, J. C.; Chen, Y.; Mohammad, T. A.; Chen, Y.; Fedor, H. L.; et al. Ar-V7 and Resistance to Enzalutamide and Abiraterone in Prostate Cancer. *N. Engl. J. Med.* **2014**, *371*, 1028−1038.

(7) Dong, L.; Zieren, R. C.; Xue, W.; de Reijke, T. M.; Pienta, K. J. Metastatic Prostate Cancer Remains Incurable, Why? *Asian J. Urol.* **2019**, *6*, 26−41.

(8) Mangadlao, J. D.; Wang, X.; McCleese, C.; Escamilla, M.; Ramamurthy, G.; Wang, Z.; Govande, M.; Basilion, J. P.; Burda, C. Prostate-Specific Membrane Antigen Targeted Gold Nanoparticles for Theranostics of Prostate Cancer. *ACS Nano* **2018**, *12*, 3714−3725.

(9) Niaz, M. O.; Sun, M.; Ramirez-Fort, M. K.; Niaz, M. J. Prostate-Specific Membrane Antigen Based Antibody-Drug Conjugates for Metastatic Castration-Resistance Prostate Cancer. *Cureus* **2020**, *12*, No. e7147.
(10) Israeli, R. S.; Powell, C. T.; Corr, J. G.; Fair, W. R.; Heston, W. D. Expression of the Prostate-Specific Membrane Antigen. *Cancer Res.* **1994**, *54*, 1807−1811.
(11) Lv, Q.; Yang, J.; Zhang, R.; Yang, Z.; Yang, Z.; Wang, Y.; Xu, Y.; He, Z. Prostate-Specific Membrane Antigen Targeted Therapy of Prostate Cancer Using a Dupa-Paclitaxel Conjugate. *Mol. Pharm.* **2018**, *15*, 1842−1852.
(12) Wright, G. L., Jr.; Mayer Grob, B.; Haley, C.; Grossman, K.; Newhall, K.; Petrylak, D.; Troyer, J.; Konchuba, A.; Schellhammer, P. F.; Moriarty, R. Upregulation of Prostate-Specific Membrane Antigen after Androgen-Deprivation Therapy. *Urology* **1996**, *48*, 326−334.
(13) Chang, S. S. Overview of Prostate-Specific Membrane Antigen. *Rev. Urol.* **2004**, *6*, S13−S18.
(14) Rajasekaran, S. A.; Anilkumar, G.; Oshima, E.; Bowie, J. U.; Liu, H.; Heston, W.; Bander, N. H.; Rajasekaran, A. K. A Novel Cytoplasmic Tail Mxxxl Motif Mediates the Internalization of Prostate-Specific Membrane Antigen. *Mol. Biol. Cell* **2003**, *14*, 4835−4845.
(15) Dorff, T. B.; Fanti, S.; Farolfi, A.; Reiter, R. E.; Sadun, T. Y.; Sartor, O. The Evolving Role of Prostate-Specific Membrane Antigen-Based Diagnostics and Therapeutics in Prostate Cancer. *Am. Soc. Clin. Oncol. Educ. Book* **2019**, *39*, 321−330.
(16) Giesel, F. L.; Sterzing, F.; Schlemmer, H. P.; Holland-Letz, T.; Mier, W.; Rius, M.; Afshar-Oromieh, A.; Kopka, K.; Debus, J.; Haberkorn, U.; et al. Intra-Individual Comparison of (68)Ga-Psma-11-Pet/Ct and Multi-Parametric Mr for Imaging of Primary Prostate Cancer. *Eur. J. Nucl. Med. Mol. Imag.* **2016**, *43*, 1400−1406.
(17) Schwarzenboeck, S. M.; Rauscher, I.; Bluemel, C.; Fendler, W. P.; Rowe, S. P.; Pomper, M. G.; Asfhar-Oromieh, A.; Herrmann, K.; Eiber, M. Psma Ligands for Pet Imaging of Prostate Cancer. *J. Nucl. Med.* **2017**, *58*, 1545−1552.
(18) Kelly, J.; Amor-Coarasa, A.; Nikolopoulou, A.; Kim, D.; Williams, C., Jr.; Ponnala, S.; Babich, J. W. Synthesis and Pre-Clinical Evaluation of a New Class of High-Affinity (18)F-Labeled Psma Ligands for Detection of Prostate Cancer by Pet Imaging. *Eur. J. Nucl. Med. Mol. Imag.* **2017**, *44*, 647−661.
(19) Pan, M.-H.; Gao, D.-W.; Feng, J.; He, J.; Seo, Y.; Tedesco, J.; Wolodzko, J. G.; Hasegawa, B. H.; Franc, B. L. Biodistributions of 177lu- and 111in-Labeled 7e11 Antibodies to Prostate-Specific Membrane Antigen in Xenograft Model of Prostate Cancer and Potential Use of 111in-7e11 as a Pre-Therapeutic Agent for 177lu-7e11 Radioimmunotherapy. *Mol. Imag. Biol.* **2009**, *11*, 159−166.
(20) Troyer, J. K.; Beckett, M. L.; Wright, G. L., Jr. Location of Prostate-Specific Membrane Antigen in the Lncap Prostate Carcinoma Cell Line. *Prostate* **1997**, *30*, 232−242.
(21) Horoszewicz, J. S.; Kawinski, E.; Murphy, G. P. Monoclonal Antibodies to a New Antigenic Marker in Epithelial Prostatic Cells and Serum of Prostatic Cancer Patients. *Anticancer Res.* **1987**, *7*, 927−935.
(22) Milowsky, M. I.; Galsky, M. D.; Morris, M. J.; Crona, D. J.; George, D. J.; Dreicer, R.; Tse, K.; Petruck, J.; Webb, I. J.; Bander, N. H.; et al. Phase 1/2 Multiple Ascending Dose Trial of the Prostate-Specific Membrane Antigen-Targeted Antibody Drug Conjugate Mln2704 in Metastatic Castration-Resistant Prostate Cancer. *Urol. Oncol.* **2016**, *34*, 530.e515−530.e521.
(23) Banerjee, S. R.; Kumar, V.; Lisok, A.; Plyku, D.; Nováková, Z.; Brummet, M.; Wharram, B.; Barinka, C.; Hobbs, R.; Pomper, M. G. Evaluation of (111)in-Dota-5d3, a Surrogate Spect Imaging Agent for Radioimmunotherapy of Prostate-Specific Membrane Antigen. *J. Nucl. Med.* **2019**, *60*, 400−406.
(24) Nováková, Z.; Foss, C. A.; Copeland, B. T.; Morath, V.; Baranová, P.; Havlínová, B.; Skerra, A.; Pomper, M. G.; Barinka, C. Novel Monoclonal Antibodies Recognizing Human Prostate-Specific Membrane Antigen (Psma) as Research and Theranostic Tools. *Prostate* **2017**, *77*, 749−764.
(25) Hapuarachchige, S.; Huang, C. T.; Donnelly, M. C.; Bařinka, C.; Lupold, S. E.; Pomper, M. G.; Artemov, D. Cellular Delivery of Bioorthogonal Pretargeting Therapeutics in Psma-Positive Prostate Cancer. *Mol. Pharm.* **2020**, *17*, 98−108.
(26) Kupchan, S. M.; Komoda, Y.; Court, W. A.; Thomas, G. J.; Smith, R. M.; Karim, A.; Gilmore, C. J.; Haltiwanger, R. C.; Bryan, R. F. Tumor inhibitors. LXXIII. Maytansine, a Novel Antileukemic Ansa Macrolide from Maytenus Ovatus. *J. Am. Chem. Soc.* **1972**, *94*, 1354−1356.
(27) Peddi, P. F.; Hurvitz, S. A. Trastuzumab Emtansine: The First Targeted Chemotherapy for Treatment of Breast Cancer. *Future Oncol.* **2013**, *9*, 319−326.
(28) Kupchan, S. M.; Komoda, Y.; Branfman, A. R.; Sneden, A. T.; Court, W. A.; Thomas, G. J.; Hintz, H. P. J.; Smith, R. M.; Karim, A.; Howie, G. A.; et al. Tumor inhibitors. 122. The Maytansinoids. Isolation, Structural Elucidation, and Chemical Interrelation of Novel Ansa Macrolides. *J. Org. Chem.* **1977**, *42*, 2349−2357.
(29) Lopus, M. Antibody-Dm1 Conjugates as Cancer Therapeutics. *Canc. Lett.* **2011**, *307*, 113−118.
(30) Lopus, M.; Oroudjev, E.; Wilson, L.; Wilhelm, S.; Widdison, W.; Chari, R.; Jordan, M. A. Maytansine and Cellular Metabolites of Antibody-Maytansinoid Conjugates Strongly Suppress Microtubule Dynamics by Binding to Microtubules. *Mol. Cancer Ther.* **2010**, *9*, 2689−2699.
(31) Rong, L.; Zhou, S.; Liu, X.; Li, A.; Jing, T.; Liu, X.; Zhang, Y.; Cai, S.; Tang, X. Trastuzumab-Modified Dm1-Loaded Nanoparticles for Her2(+) Breast Cancer Treatment: An in Vitro and in Vivo Study. *Artif. Cells, Nanomed., Biotechnol.* **2018**, *46*, 1708−1718.
(32) Zimmerman, M. E.; Meyer, A. R.; Rowe, S. P.; Gorin, M. A. Imaging of Prostate Cancer with Positron Emission Tomography. *Clin. Adv. Hematol. Oncol.* **2019**, *17*, 455−463.
(33) Rowe, S. P.; Drzezga, A.; Neumaier, B.; Dietlein, M.; Gorin, M. A.; Zalutsky, M. R.; Pomper, M. G. Prostate-Specific Membrane Antigen-Targeted Radiohalogenated Pet and Therapeutic Agents for Prostate Cancer. *J. Nucl. Med.* **2016**, *57*, 90S−96S.
(34) Current, K.; Meyer, C.; Magyar, C. E.; Mona, C. E.; Almajano, J.; Slavik, R.; Stuparu, A. D.; Cheng, C.; Dawson, D. W.; Radu, C. G.; et al. Investigating Psma-Targeted Radioligand Therapy Efficacy as a Function of Cellular Psma Levels and Intratumoral Psma Heterogeneity. *Clin. Cancer Res.* **2020**, *26*, 2946−2955.
(35) Müller, C.; Umbricht, C. A.; Gracheva, N.; Tschan, V. J.; Pellegrini, G.; Bernhardt, P.; Zeevaart, J. R.; Koster, U.; Schibli, R.; van der Meulen, N. P. Terbium-161 for Psma-Targeted Radionuclide Therapy of Prostate Cancer. *Eur. J. Nucl. Med. Mol. Imag.* **2019**, *46*, 1919−1930.
(36) Phillips, G. D. L.; Li, G.; Dugger, D. L.; Crocker, L. M.; Parsons, K. L.; Mai, E.; Blattler, W. A.; Lambert, J. M.; Chari, R. V.; Lutz, R. J.; et al. Targeting Her2-Positive Breast Cancer with Trastuzumab-Dm1, an Antibody-Cytotoxic Drug Conjugate. *Cancer Res.* **2008**, *68*, 9280−9290.
(37) Machulkin, A. E.; Ivanenkov, Y. A.; Aladinskaya, A. V.; Veselov, M. S.; Aladinskiy, V. A.; Beloglazkina, E. K.; Koteliansky, V. E.; Shakhbazyan, A. G.; Sandulenko, Y. B.; Majouga, A. G. Small-Molecule Psma Ligands. Current State, Sar and Perspectives. *J. Drug Target.* **2016**, *24*, 679−693.
(38) Hapuarachchige, S.; Kato, Y.; Artemov, D. Bioorthogonal Two-Component Drug Delivery in Her2(+) Breast Cancer Mouse Models. *Sci. Rep.* **2016**, *6*, 24298.
(39) Hapuarachchige, S.; Zhu, W.; Kato, Y.; Artemov, D. Bioorthogonal, Two-Component Delivery Systems Based on Antibody and Drug-Loaded Nanocarriers for Enhanced Internalization of Nanotherapeutics. *Biomaterials* **2014**, *35*, 2346−2354.
(40) Haun, J. B.; Devaraj, N. K.; Hilderbrand, S. A.; Lee, H.; Weissleder, R. Bioorthogonal Chemistry Amplifies Nanoparticle Binding and Enhances the Sensitivity of Cell Detection. *Nat. Nanotechnol.* **2010**, *5*, 660−665.
(41) Galsky, M. D.; Eisenberger, M.; Moore-Cooper, S.; Kelly, W. K.; Slovin, S. F.; DeLaCruz, A.; Lee, Y.; Webb, I. J.; Scher, H. I. Phase I Trial of the Prostate-Specific Membrane Antigen-Directed

https://dx.doi.org/10.1021/acs.molpharmaceut.0c00457
Mol. Pharmaceutics 2020, 17, 3392−3402

Immunoconjugate Mln2704 in Patients with Progressive Metastatic Castration-Resistant Prostate Cancer. *J. Clin. Oncol.* **2008**, *26*, 2147−2154.
(42) Kobayashi, H.; Choyke, P. L. Super Enhanced Permeability and Retention (Supr) Effects in Tumors Following near Infrared Photoimmunotherapy. *Nanoscale* **2016**, *8*, 12504−12509.
(43) Nakamura, Y.; Mochida, A.; Choyke, P. L.; Kobayashi, H. Nanodrug Delivery: Is the Enhanced Permeability and Retention Effect Sufficient for Curing Cancer? *Bioconjugate Chem.* **2016**, *27*, 2225−2238.
(44) Lee, S. Y.; Ju, M. K.; Jeon, H. M.; Jeong, E. K.; Lee, Y. J.; Kim, C. H.; Park, H. G.; Han, S. I.; Kang, H. S. Regulation of Tumor Progression by Programmed Necrosis. *Oxid. Med. Cell. Longevity* **2018**, *2018*, 3537471.
(45) Tomes, L.; Emberley, E.; Niu, Y.; Troup, S.; Pastorek, J.; Strange, K.; Harris, A.; Watson, P. H. Necrosis and Hypoxia in Invasive Breast Carcinoma. *Breast Canc. Res. Treat.* **2003**, *81*, 61−69.
(46) Cheville, J. C.; Lohse, C. M.; Zincke, H.; Weaver, A. L.; Blute, M. L. Comparisons of Outcome and Prognostic Features among Histologic Subtypes of Renal Cell Carcinoma. *Am. J. Surg. Pathol.* **2003**, *27*, 612−624.
(47) Jin, S.; DiPaola, R. S.; Mathew, R.; White, E. Metabolic Catastrophe as a Means to Cancer Cell Death. *J. Cell Sci.* **2007**, *120*, 379−383.

https://dx.doi.org/10.1021/acs.molpharmaceut.0c00457
Mol. Pharmaceutics 2020, 17, 3392−3402

molecular pharmaceutics

Article

Cite This: Mol. Pharmaceutics 2020, 17, 98−108

pubs.acs.org/molecularpharmaceutics

Cellular Delivery of Bioorthogonal Pretargeting Therapeutics in PSMA-Positive Prostate Cancer

Sudath Hapuarachchige,*[,†] Colin T. Huang,[†] Madeline C. Donnelly,[†] Cyril Bařinka,[‡] Shawn E. Lupold,[§] Martin G. Pomper,[†,§,∥] and Dmitri Artemov*[,†,∥]

[†]The Russell H. Morgan Department of Radiology and Radiological Science, The Johns Hopkins University School of Medicine, 720 Rutland Avenue, Baltimore, Maryland 21205, United States

[‡]Laboratory of Structural Biology, Institute of Biotechnology of the Czech Academy of Sciences, Prumyslova 595, Vestec 252 50, Czech Republic

[§]The James Buchanan Brady Urologic Institute and Department of Urology, Johns Hopkins School of Medicine, 600 N. Wolfe St., Baltimore, Maryland 21287, United States

[∥]Department of Oncology, The Sidney Kimmel Comprehensive Cancer Center, The Johns Hopkins University School of Medicine, 401 N. Broadway, Baltimore, Maryland 21231, United States

Supporting Information

ABSTRACT: Prostate cancer is primarily fatal after it becomes metastatic and castration-resistant despite novel combined hormonal and chemotherapeutic regimens. Hence, new therapeutic concepts and drug delivery strategies are urgently needed for the eradication of this devastating disease. Here we report the highly specific, *in situ* click chemistry driven pretargeted delivery of cytotoxic drug carriers to PSMA(+) prostate cancer cells. Anti-PSMA 5D3 mAb and its $F(ab')_2$ fragments were functionalized with *trans*-cyclooctene (TCO), labeled with a fluorophore, and used as pretargeting components. Human serum albumin (ALB) was loaded with the DM1 antitubulin agent, functionalized with PEGylated tetrazine (PEG_4-Tz), labeled with a fluorophore, and used as the drug delivery component. The internalization kinetics of components and the therapeutic efficacy of the pretargeted click therapy were studied in PSMA(+) PC3-PIP and PSMA(−) PC3-Flu control cells. The $F(ab')_2$ fragments were internalized faster than 5D3 mAb in PSMA(+) PC3-PIP cells. In the two-component pretargeted imaging study, both components were colocalized in a perinuclear location of the cytoplasm of PC3-PIP cells. Better colocalization was achieved when 5D3 mAb was used as the pretargeting component. Consecutively, the *in vitro* cell viability study shows a significantly higher therapeutic effect of click therapy in PC3-PIP cells when 5D3 mAb was used for pretargeting, compared to its $F(ab')_2$ derivative. 5D3 mAb has a longer lifetime on the cell surface, when compared to its $F(ab')_2$ analogue, enabling efficient cross-linking with the drug delivery component and increased efficacy. Pretargeting and drug delivery components were cross-linked via multiple bioorthogonal click chemistry reactions on the surface of PSMA(+) PC cells forming nanoclusters, which undergo fast cellular internalization and intracellular transport to perinuclear locations.

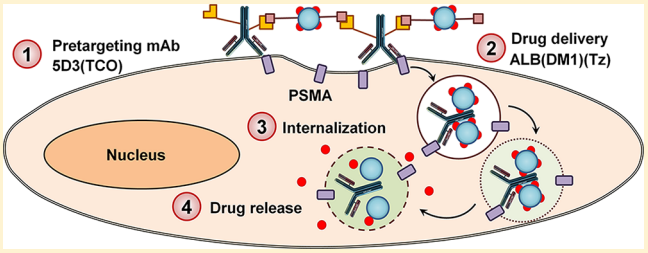

KEYWORDS: *pretargeted therapy, drug delivery, PSMA(+) prostate cancer, nanomedicine, bioorthogonal click chemistry*

1. INTRODUCTION

Prostate cancer (PC) is the most common noncutaneous malignancy in American men.[1−3] Over 170 000 new cases of PC are diagnosed, and approximately 30 thousand patients die from PC each year in the US.[4] Conventional treatments such as surgery, radiation, and androgen deprivation are effective; however, PC is essentially incurable once it becomes metastatic and castration-resistant.[5−9] That outcome persists despite the approval of several new drugs and combined hormonal and chemotherapeutic regimens.[10,11] Novel therapeutic approaches and cancer-specific drug delivery strategies are urgently needed for the improved management and eventual complete eradication of this devastating disease.[12−14]

The prostate-specific membrane antigen (PSMA) is a type II membrane protein that is highly expressed in aggressive PC.[15−18] Due to the cell-surface and cancer-specific nature of PSMA, and its rapid cellular internalization and recycling kinetics, PSMA is a leading target for primary and metastatic PC diagnosis, imaging, and therapy.[19−21] PSMA has glutamate carboxypeptidase activity and can be targeted with small-molecule substrate analogues as well as engineered peptides, aptamers, and antibodies.[22−31] Nanosize hyperbranched

Received: July 23, 2019
Revised: November 22, 2019
Accepted: November 25, 2019
Published: December 16, 2019

DOI: 10.1021/acs.molpharmaceut.9b00788
Mol. Pharmaceutics 2020, 17, 98−108

Scheme 1. Synthesis of 5D3 mAb and Its F(ab′)$_2$-Based Pretargeting Components[a]

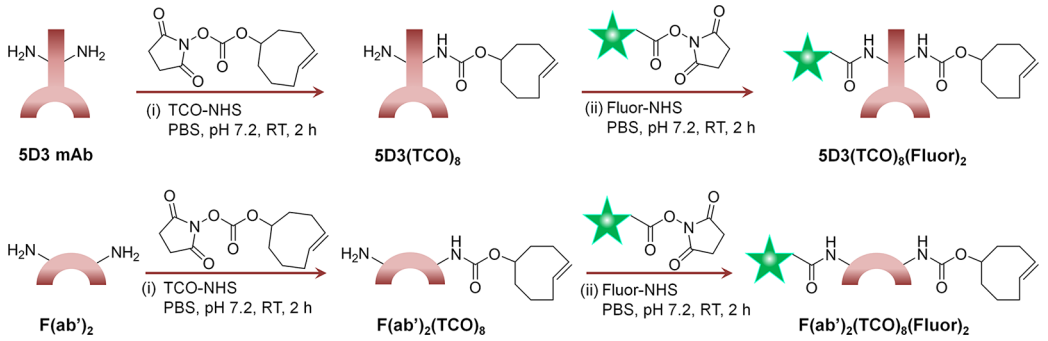

[a](i) 5D3 mAb was treated with TCO-NHS to obtain 5D3(TCO)$_8$ and then (ii) labeled with a suitable fluorophore to obtain the final product, 5D3(TCO)$_8$(Fluor)$_2$. The same synthetic route was followed starting with F(ab′)$_2$ of 5D3 to obtain (i) F(ab′)$_2$(TCO)$_8$ and (ii) F(ab′)$_2$(TCO)$_8$(Fluor)$_2$. Subscripted numbers in the formulas indicate the number of TCO or fluorophores attached per biomolecule.

polymers conjugated with PSMA-specific small molecules, peptides, and anti-PSMA antibodies have also been successfully studied as therapeutic delivery platforms targeting PSMA(+) PC in mouse models.[32] Anti-PSMA antibodies typically enhance the internalization of PSMA and can be used for the delivery of isotopes and drugs targeting PSMA(+) prostate cancers.[33] Only two monoclonal antibodies, J591 and 7E11, have moved to clinical trials, and radiolabeled variants of J591 have progressed to Phase II.[34−36] The 5D3 mAb is a novel anti-PSMA mAb, recently developed and used for imaging PC.[37] In preclinical binding and imaging studies, the 5D3 mAb has demonstrated higher PSMA binding affinity when compared to J591.[37,38]

Antibody−drug conjugate (ADC) drug delivery systems have shown promising results in cancer therapy over recent decades.[39−42] Target specificity and the use of a minimum amount of highly cytotoxic chemotherapeutics increase ADC efficacy.[43] Moving forward, pretargeted drug delivery can be an even more effective strategy by circumventing the use of highly cytotoxic chemotherapeutics with significant off-target effects in cancer treatment.[44,45] We have previously developed a bioorthogonal pretargeted two-component drug delivery system driven by *trans*-cyclooctene (TCO) and PEGylated tetrazine (PEG$_4$-Tz) *in situ* click chemistry for specific delivery of therapeutics to HER2(+) breast cancer.[44] This strategy can be applied to other cancer types such as PC, which overexpress cancer-specific PSMA on the cell surface.

The *trans*-cyclooctene-tetrazine (TCO-Tz) click chemistry is a strain-promoted reaction that does not require catalysts and can proceed under mild conditions. TCO-Tz click chemistry is ideal for biological applications, as it can be performed under physiological conditions and releases no toxic byproducts.[46,47] This inverse-electron demand Diels−Alder (IEDDA) cycloaddition reaction exhibits exceptional kinetics (k > 100 000 M^{-1} s^{-1}) and chemoselectivity. We have utilized this bioorthogonal click reaction for *in situ* conjugations of two components in physiological conditions to enhance the cellular internalization of drugs, and this strategy has shown enhanced therapeutic efficacy in preclinical breast cancer models. In this study, we have applied and extended the strategy of bioorthogonal pretargeted drug delivery to PSMA(+) PC using novel functionalized 5D3 mAb or its F(ab′)$_2$ domains as the pretargeting component, and the highly cytotoxic drug, mertansine (DM1)-loaded human serum albumin (ALB), as the drug delivery component. This approach has demonstrated high efficacy in PSMA(+) PC cells.

2. MATERIALS AND METHODS

2.1. Antibody, Chemotherapeutics, and Chemicals. 5D3 mAb in PBS with 0.02% NaN_3 was prepared as described previously and used after buffer exchange to pure BupH phosphate buffered saline (PBS).[37] Mertansine (DM1) was purchased from Abcam, Inc. The amine-reactive linkers, TCO-NHS and methyltetrazine-PEG$_4$-NHS esters, were purchased from Sigma-Aldrich Corp. and KeraFast, Inc., respectively. Sulfo-SMCC heterobifunctional crosslinker, NHS esters of fluorophores, and Dulbecco's phosphate-buffered saline (DPBS) were purchased from ThermoFisher, Inc.

2.2. 5D3 mAb Fragmentation. The F(ab′)$_2$ fragments of 5D3 mAb were prepared using the Pierce Mouse IgG1 Fab and F(ab′)$_2$ Preparation Kit (Thermo Scientific) following the manufacturer's protocol. Briefly, 5D3 antibody (3 mg in 0.5 mL of PBS) was digested for 24 h at 37 °C in mouse IgG1 digestion buffer with the provided Immobilized Ficin resin in the presence of cysteine·HCl (0.5 mL of 0.7 mg/mL). Digested F(ab′)$_2$ fragments were separated from the resin by centrifugation (5000*g*, 1 min) followed by 3 separate washes with provided protein A binding buffer to collect a total of 2.0 mL. The F(ab′)$_2$ fragments were purified using a Nab protein A plus spin column and protein A binding buffer.

2.3. Synthesis of Pretargeting Components. The 5D3 mAb or F(ab′)$_2$ fragments (2 mg in 500 μL of PBS) were treated with TCO-NHS ester (250 mol equiv in 10−20 μL of anhydrous DMSO) and incubated for 2 h. The 2−4% DMSO/PBS reaction mixture was initially cloudy, and TCO-NHS ester was not completely soluble. However, the reaction mixture was clear after 1-2 h, and excess TCO-NHS and byproducts were removed by ultrafiltration (Scheme 1). The product was further purified by size-exclusion column chromatography (SEC). The comparatively higher equivalent of TCO-NHS ester was required for this reaction, possibly due to poor solubility. The number of TCO groups attached per antibody or antibody fragments was determined based on the change of molecular weight measured by Voyager DE-STR MALDI-TOF mass spectrometer (Figure S1). The change of molecular weight corresponds to the total molecular weights of TCO groups attached to 5D3 or F(ab′)$_2$.

The number of groups attached is denoted as the subscripted number in the formulas. The hydrodynamic

DOI: 10.1021/acs.molpharmaceut.9b00788
Mol. Pharmaceutics 2020, 17, 98−108

Scheme 2. Synthesis of the Albumin (ALB)-Based Drug delivery Component[a]

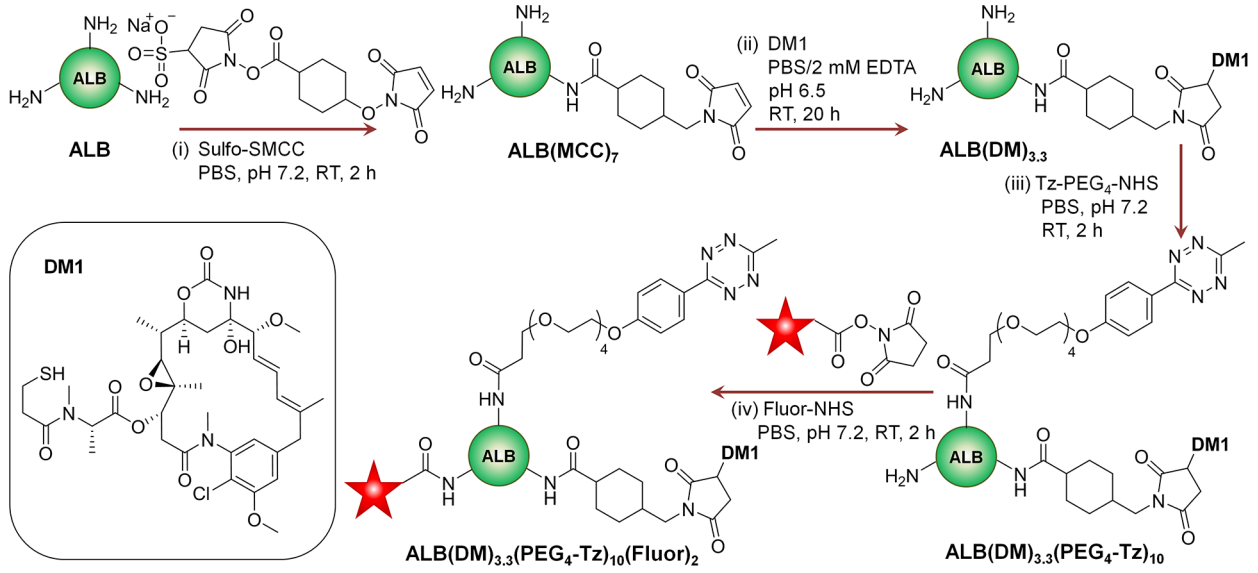

[a](i) ALB was treated with the sulfo-SMCC bifunctional linker to obtain ALB(MCC)$_7$. (ii) It was conjugated with DM1 drug molecules, and the resultant ALB(DM1)$_{3.3}$ was treated with (iii) NHS-PEG$_4$-Tz ester to obtain ALB(DM1)$_{3.3}$(PEG$_4$-Tz)$_{10}$. (iv) It was labeled with a suitable fluorophore to obtain the final product, ALB(DM1)$_{3.3}$(PEG$_4$-Tz)$_{10}$(Fluor)$_2$. The subscripted numbers in the formulas indicate the number of MCC, DM1, PEG$_4$-Tz groups, or fluorophores attached per protein.

diameter of components was measured by dynamic light scattering (DLS) using a Nano-ZS90 (Malvern Instruments, U.K.) Zetasizer (Figure S2). For imaging experiments and flow cytometry, the native 5D3 antibody, F(ab′)$_2$, and functionalized 5D3(TCO)$_8$, and F(ab′)$_2$(TCO)$_8$ (~500 μL of 1 mg/mL in PBS) were labeled with AlexaFluor 488 or Cy5 by adding AlexaFluor 488 NHS ester or Cy5-NHS ester (10−20 mol equiv in 10 μL of anhydrous DMSO) and stirred for 2 h, and excess dye was removed by ultrafiltration. A fraction of fluorescent 5D3(AF-488)$_2$ (250 μg in 250 μL in PBS) was further labeled with a low-pH fluorescence indicator, pHrodo, by adding pHrodo-NHS (20−50 mol equiv in 10 μL of anhydrous DMSO). After stirring for 2 h, the excess dye was removed by ultrafiltration. After fluorescence labeling, all products were further purified by SEC chromatography. The degree of fluorescence labeling was determined following the manufacturer's protocol.

2.4. Synthesis of Delivery Components. Human serum albumin (ALB, 20 mg in 4 mL of PBS) was treated with a 10-fold molar excess of sulfosuccinimidyl 4-(*N*-maleimidomethyl)cyclohexane-1-carboxylate (Sulfo-SMCC) in dry DMSO and stirred for 2 h (Scheme 2). The excess SMCC and byproducts were removed by ultrafiltration, and the product was further purified by size-exclusion chromatography (SEC). The ALB functionalized by SMCC (10 mg in 2 mL of PBS with 2 mM EDTA, pH 6.5) was treated with mertansine (DM1, 10 mol equiv in 10 μL of anhydrous DMSO) and stirred for 20 h at room temperature. The excess DM1 was removed by ultrafiltration, and the product, ALB(DM1)$_{3.3}$, was further purified by SEC chromatography. ALB(DM1)$_{3.3}$ (5 mg in 1 mL of PBS) was functionalized with PEG$_4$-Tz by adding methyltetrazine-PEG$_4$-NHS ester (100 mol equiv in 10 μL of anhydrous DMSO) and stirring for 2 h. The resulting product ALB(DM1)$_{3.3}$(PEG$_4$-Tz)$_{10}$ was purified by ultrafiltration, followed by SEC chromatography. The product, ALB(DM1)$_{3.3}$(PEG$_4$-Tz)$_{10}$ (3 mg in 1 mL of PBS), was treated with rhodamine-NHS ester or AlexaFluor 488 NHS ester (20 mol equiv in 10−20 μL of anhydrous DMSO) and stirred for 2 h to obtain ALB(DM1)$_{3.3}$(PEG$_4$-Tz)$_{10}$(Rhod)$_2$ and ALB(DM1)$_{3.3}$(PEG$_4$-Tz)$_{10}$(AF-488)$_2$. The product was finally purified by ultrafiltration followed by SEC chromatography. After each step, the molecular weights of intermediates and final products were determined using the Voyager DE-STR MALDI-TOF mass spectrometer. The degree of MCC linker conjugation, DM1 drug load, and PEG$_4$-Tz functionalization were determined based on the change of molecular weights (Figure S1) and is denoted as subscripts in formulas. The degree of fluorophore labeling was determined following the manufacturer's protocol.

2.5. Purification of the Products. After each step of the synthesis, the excess small molecular reagents and byproducts were removed by Amicon ultrafiltration using 15 mL, 30 kDa MWCO units (for ≥2 mg samples) or 0.5 mL, 30 kDa MWCO units (for ≤2 mg samples). The products were further purified by SEC chromatography by the Waters binary pump/dual absorbance HPLC system equipped with a YMC-Pack Diol-300 (300 × 8.0 mm I.D.; particle size, 5 μm; pore size, 30 nm) size-exclusion column, using 0.1 M PBS with 0.2 M NaCl (pH 7.2) as the mobile phase.

2.6. Cells. PSMA(+) PC3-PIP and PSMA(−) PC3-Flu cells were used to prove the strategy in PSMA(+) PC. Cells were grown in RPMI 1640 medium supplemented with 10% FBS and 1% penicillin−streptomycin and maintained in a humidified incubator at 37 °C with 5% CO_2. Cells were confirmed to be free of mycoplasma contamination.

2.7. Time-Dependent Internalization of Pretargeting Components. PC3-PIP or PC3-Flu cells were seeded in 4-well chamber slides (0.2 million cells per chamber) and grown for 24−48 h to 80−90% confluency. Each chamber was treated with 150 μL of 20 μg/mL of 5D3(AF-488)$_2$ or F(ab′)$_2$(AF-488)$_2$ and incubated at 37 °C under CO_2 and humidity-controlled conditions. Chambers at each time point (15 min, 1, 6, 24 h) were washed with Dulbecco's phosphate buffered saline (DPBS) for 5 min and fixed using 4% paraformaldehyde

DOI: 10.1021/acs.molpharmaceut.9b00788
Mol. Pharmaceutics 2020, 17, 98−108

(PFA) for 10 min on ice. The nuclei were counterstained using Hoechst 33342 and wet mounted. Images were taken using an inverted confocal microscope and analyzed using dedicated software developed in the IDL and MatLab environment. Briefly, the program searches for the cell membrane-extracellular medium interface using a user-defined coarse outline of the cell membrane. The algorithm provides the precise position of the plasma membrane based on the intensity gradient analysis of the images. Membrane areas with low fluorescence signals are interpolated using neighboring regions with a high fluorescence intensity. Integral fluorescence localized to the membrane (within the search radius from the interface) and the integral internalized signal within the space enclosed within the membrane was evaluated for each cell within the field of view. The measured values are exported in a tabular format.

2.8. mAb Internalization Inhibition Study. PC3-PIP cells (0.2 million/chamber) were seeded in 4-well chamber slides and grown for 24−48 h to 80−90% confluency. Each chamber was treated with 150 μL of 2 μg/mL 5D3(AF-488)$_2$ in DPBS in the presence of endocytosis inhibitors, chlorpromazine hydrochloride (10 μg/mL), methyl-β-cyclodextrin (5 mM), or Nocodazole (20 μM). Two control experiments were performed treating PC3-PIP cells with 2 μg/mL 5D3(AF-488) alone and incubated at 4 and 37 °C.[48] After 1 h, cells were washed with DPBS and fixed with 4% PFA in PBS. After the nuclear counterstaining by Hoechst 33342, the slide was wet mounted, and cells were imaged using a Zeiss AxioObserver confocal fluorescence microscope with an LSM700 confocal module.

2.9. Flow Cytometry Analysis. For the determination of PSMA expression levels, PC3-PIP and PC3-Flu cells were seeded in a 6-well plate (0.4 million/well) and grown for 24 h to ∼90% confluency. Then cells were treated with 5D3(Cy5)$_2$ or F(ab′)$_2$(Cy5)$_2$ (20 μg/mL) and incubated for 30 min at 4 °C. Cells were washed once using DPBS and harvested by trypsinization. Cell pellets were resuspended in buffer and fixed by 4% PFA for flow cytometry. To prove the click delivery, PSMA(+) PC3-PIP and PSMA(−) PC3-Flu cells were seeded in a 6-well plate (0.4 million/well) and grown for 24 h to ∼90% confluency. Then, cells in each well were treated with one of the reactive pretargeting components, 5D3-(TCO)$_8$(Cy5)$_2$, F(ab′)$_2$(TCO)$_8$(Cy5)$_2$, or unreactive 5D3-(Cy5)$_2$, and F(ab′)$_2$(Cy5)$_2$ (20 μg/mL), and incubated for 20 min at 37 °C. Cells were washed once with DPBS, treated with a drug delivery component, ALB(DM1)$_{3.3}$(PEG$_4$-Tz)$_{10}$(AF-488)$_2$ (50 μg/mL in DPBS), and incubated for 30 min at 37 °C. Then, the treating solution was replaced by fresh media, and cells were incubated for an additional 1.5−2 h. Cells were washed once using DPBS and harvested by trypsinization. Cell pellets were resuspended in buffer and fixed by 4% PFA. Cells were analyzed on a BD LSR II Flow Cytometer using red (633 nm) and blue (488 nm) lasers for Cy5 and AlexaFluor 488, respectively. Histograms for PSMA expression levels and fluorescence density plots for each click delivery tests are presented in Figure 2.

2.10. *In Vitro* Two-Component Delivery Imaging Study. PC3-PIP and PC3-Flu cells grown in 4-well chamber slides were treated with 5D3(TCO)$_8$(AF-488)$_2$ or F-(ab′)$_2$(TCO)$_8$(AF-488)$_2$ (150 μL of 20 μg/mL in each well) and incubated at 37 °C for 30 min, and unbound pretargeting components were washed by DPBS. Cells were then treated with ALB(DM1)$_{3.3}$(PEG$_4$-Tz)$_{10}$(Rhod)$_2$ (150 μL of 50 μg/mL in DPBS) at 37 °C for 30 min. After the washing step, DPBS was replaced by the growth medium, and the incubation was continued for 30 min, 1, 2, and 4 h. After each time point, selected chambers of cells were fixed by 4% PFA for 20 min at 4 °C and washed with deionized H_2O. Fixed slides were imaged using the Zeiss AxioObserver confocal fluorescence microscope with an LSM700 confocal module and analyzed using NIH ImageJ.

2.11. *In Vitro* Study of Pretargeted Therapy. PC3-PIP or PC3-Flu cells (2000 cells/well in 200 μL of a medium) were seeded in a 96-well plate and incubated at 37 °C for 24 h. Cultured cells were treated with or without modified or unmodified 5D3 or its F(ab′)$_2$ fragments (20 μg/mL in 100 μL of DPBS) and incubated at 37 °C for 20 min. Cells were washed with DPBS and incubated for 2 h with or without the drug delivery component ALB(DM1)$_{3.3}$(PEG$_4$-Tz)$_{10}$(Rhod)$_2$ or with DM1 (1.5 μg/mL in 100 μL of DPBS). After treatment, cells were washed with DPBS and resupplied with fresh media. After the incubation for 48 h, the cell viability was determined using the WST-8 assay, following the manufacturer's protocol. Briefly, cells in 100 μL of media were treated with 10 μL of the WST-8 reagent per well and incubated at 37 °C. After 3 h, the absorbance was measured at 450 nm. The WST-8 is tetrazolium salt, which is reduced by dehydrogenase in living cells forming a yellow formazan dye. This dye turns media into a yellow color (450 nm absorption peak). The concentration of the formazan dye in the media produced by the activities of dehydrogenases in living cells is directly proportional to the number of viable cells. The cell viability of treated cells was normalized to readings in untreated control cells, which were considered to have 100% viability.

2.12. Statistical Analysis. The *in vitro* therapeutic study was performed in triplicate per plate, and duplicate independent experiments were performed for statistical analysis. The WST-8 assay test was quadruplicated per plate, and triplicate independent experiments were carried out for the statistical analysis. The one-way analysis of variance (ANOVA) was used for the omnibus F-test, and the Scheffé's test was used for post hoc analysis (StatPlus:mac, AnalystSoft Inc., Alexandria, VA, USA). Changes in the cell viability were considered significant (p-value < 0.05) when the F value is greater than the critical value of the F-distribution.

3. RESULTS

3.1. Design and Synthesis of Components. Anti-PSMA 5D3 mAb and F(ab′)$_2$ fragments of 5D3 mAb were labeled with AlexaFluor-488 for the *in vitro* internalization experiments. For pretargeting experiments, 5D3 mAb and F(ab′)$_2$ were first functionalized with TCO bioorthogonal reactive groups. The number of TCO groups was maintained at ∼8 for both biomolecules. The second delivery component that was based on human serum ALB was functionalized by the SMCC linker and conjugated with DM1 by maleimide−thiol conjugation. It was further functionalized with tetrazine, the corresponding bioorthogonal click reactive group. The number of drug molecules and tetrazine groups was maintained at ∼3 and ∼10, respectively. Molecular weights of all intermediate and final components were measured by MALDI-TOF (Figure S1). The number of conjugated groups and drugs was determined based on the change of molecular weight, as shown in Figure S1. The sizes of components were measured by dynamic light scattering using the Zetasizer (Figure S2). Changes in size after modifications were not statistically

DOI: 10.1021/acs.molpharmaceut.9b00788
Mol. Pharmaceutics 2020, 17, 98−108

significant. For optical imaging, both mAb and ALB conjugates were labeled with rhodamine and AlexaFluor 488 fluorophores, respectively. For flow cytometry analysis, pretargeting and drug delivery components were labeled with Cy5 and AlexaFluor 488, respectively, to match with the configuration available in the FACS instrument.

3.2. Analysis of the Internalization of Pretargeting Components. The internalization of fluorescence-labeled 5D3 and $F(ab')_2$ fragments was studied *in vitro* with PSMA(+) PC3-PIP cells (Figure S3). The fluorescence intensity of internalized and cell surface-bound components was measured by a dedicated software developed in IDL and MatLab. The ratio of the internalized and membrane-bound fluorescence was reported for each cell in the field of view. Both components exhibit similar internalization rates; 75% of cell surface-bound 5D3 was internalized within 2.5 h, whereas 75% of the internalization of $F(ab')_2$ took approximately 1 h. The fluorescence intensity faded with time; however, a significant amount of the pretargeting component was retained in the cytoplasm for up to 24 h. No significant specific binding and/or internalization was detected in PSMA(−) PC3-Flu cells (data not shown).

3.3. Localization of the Pretargeting Component. $5D3(AF\text{-}488)_2(pHrodo)_2$ was used to determine the cellular microenvironment in which 5D3 mAb was localized after internalization. pHrodo red is an intracellular fluorescent pH indicator that only becomes fluorescent, at low pH (<6.5). The dye is typically used for the identification of late endosomes. After 4 h of incubation with PSMA(+) PC3-PIP cells, the intracellular compartments were bright red. This signal colocalized with the green 5D3 signal, indicating localization within the acidic late-stage endosomes (Figure 1A). Internalization was further investigated by imaging PC3-PIP cells treated with $5D3(AF\text{-}488)_2$ at 4 °C and at 37 °C in the presence of internalization inhibitors such as chloropromazine hydrochloride, which inhibits clathrin-mediated endocytosis; methyl-β-cyclodextrin, which inhibits caveolae-mediated endocytosis; and nocodazole, which is an antineoplastic agent that interferes with the polymerization of microtubules (Figure 1B). The fluorescence images of cells treated at 4 °C showed no internalization of 5D3. Despite the presence of inhibitors, 5D3 was predominantly internalized at 37 °C and localized in the cytoplasm, proving that internalization is not entirely controlled by clathrin-mediated or caveolae-mediated endocytosis, which agrees well with previously reported results.[33,49,50]

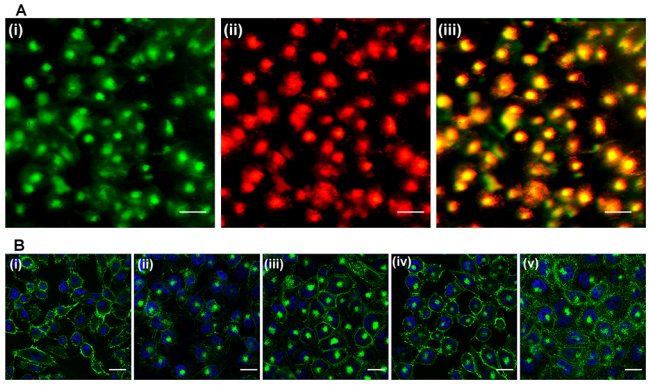

Figure 1. Internalization study of 5D3 mAb. (A) Internalization of $5D3(AF\text{-}488)_2(pHrodo)_2$, green channel (i), low-pH-activated red channel (ii), and merged image (iii) (scale bar: 100 μm). (B) Internalization of 5D3 at 4 °C (i) and 37 °C (ii) and internalization of 5D3 in the presence of internalization inhibitors, chlorpromazine hydrochloride (iii), methyl-β-cyclodextrin (iv), and nocodazole (v) (scale bar: 100 μm).

3.4. Flow Cytometric Analysis of Click Delivery. As shown in FACS histograms in Figure 2A, both $5D3(Cy5)_2$ and $F(ab')_2(Cy5)_2$ have high binding affinity in PSMA(+) PC3-PIP cells, and no accumulation was observed in PSMA(−) PC3-Flu cells. Figure 2B shows density dot plots for both Cy5 and AF-488 channels. Both pretargeting and drug delivery components accumulated in PC3-PIP cells but not in PC3-Flu cells. Reactive $5D3(TCO)_8(Cy5)_2$ and $F(ab')_2(TCO)_8(Cy5)_2$ pretargeting components and the $ALB(DM1)_{3.3}(PEG_4\text{-}Tz)_{10}(AF\text{-}488)_2$ drug carrier were used in these experiments. When the experiment was repeated using click unreactive pretargeting components (without the TCO group), $5D3(Cy5)_2$ and $F(ab')_2(Cy5)_2$, accumulation of Cy5-labeled pretargeting components was high in PC3-PIP cells and low in PC3-Flu cells, respectively (Figure 2C). The fluorescence signal corresponding to $ALB(DM1)_{3.3}(PEG_4\text{-}Tz)_{10}(AF\text{-}488)_2$ was low in both cell lines as there was no specific click reaction between the components.

3.5. Imaging Assessment of Click Delivery. Figure 3A shows images of PC3-PIP cells treated with the two-component pretargeting system. First, the pretargeting component $5D3(TCO)_8(AF\text{-}488)_2$ labeled the PSMA receptors on the cell surface. After washing the excess and unbound pretargeting components, cells were treated with the second delivery component, $ALB(PEG_4\text{-}Tz)_{10}(Rhod)_2$. Both components underwent multiple strain-promoted TCO-Tz click reactions in physiological conditions, self-assembled, and formed nanoscale clusters on the cell surface. The nanoscale clusters can efficiently internalize into the cytoplasm.[51,52]

In this experiment, colocalization of two components was observed in the cytoplasm, depicting an efficient bioorthogonal two-component drug delivery in PSMA(+) PC cells using a 5D3 mAb-based pretargeted strategy. Multichannel images were rendered in the Amira 3D software platform (Thermo Fisher) to visualize the colocalization of two components in the cells (Figure 3B). We conducted an *in vitro* control experiment using the second delivery component, $ALB(PEG_4\text{-}Tz)_{10}(Rhod)_2$, without the pretargeted step. PSMA(+) PC3-PIP cells treated with $ALB(PEG_4\text{-}Tz)_{10}(Rhod)_2$ in the absence of pretargeting $5D3(TCO)_8(AF\text{-}488)_2$, showed low accumulation of the delivery component on the cell surface or in the cytoplasm (Figure S4).

The pretargeting components, $5D3(TCO)_8(AF\text{-}488)_2$ or $F(ab')_2(TCO)_8(AF\text{-}488)_2$, and the drug-carrier component, $ALB(DM1)_{3.3}(PEG_4\text{-}Tz)_{10}(Rhod)_2$, were first used to analyze time-dependent delivery by fluorescent imaging. In this strategy, the pretargeting component-labeled cell surface PSMA receptors react with the second component via *in situ* bioorthogonal TCO-Tz click reactions. Multiple click reactions among the components form nanoscale clusters that internalize faster and more efficiently than individual components.[53] Based on the fluorescence image analysis, the time for internalization of 75% of 5D3-based pretargeting and delivery component complexes was 4 h (Figures 4 and 5). On the other hand, $F(ab')_2$-based pretargeting was significantly faster and resulted in the internalization of 75% of complexes within 2 h (Figures 6 and 7). Further analysis of fluorescence images of $F(ab')_2$-based delivery shows that a significant amount of $F(ab')_2(TCO)_8$ is dispersed in the cytoplasm without

DOI: 10.1021/acs.molpharmaceut.9b00788
Mol. Pharmaceutics 2020, 17, 98−108

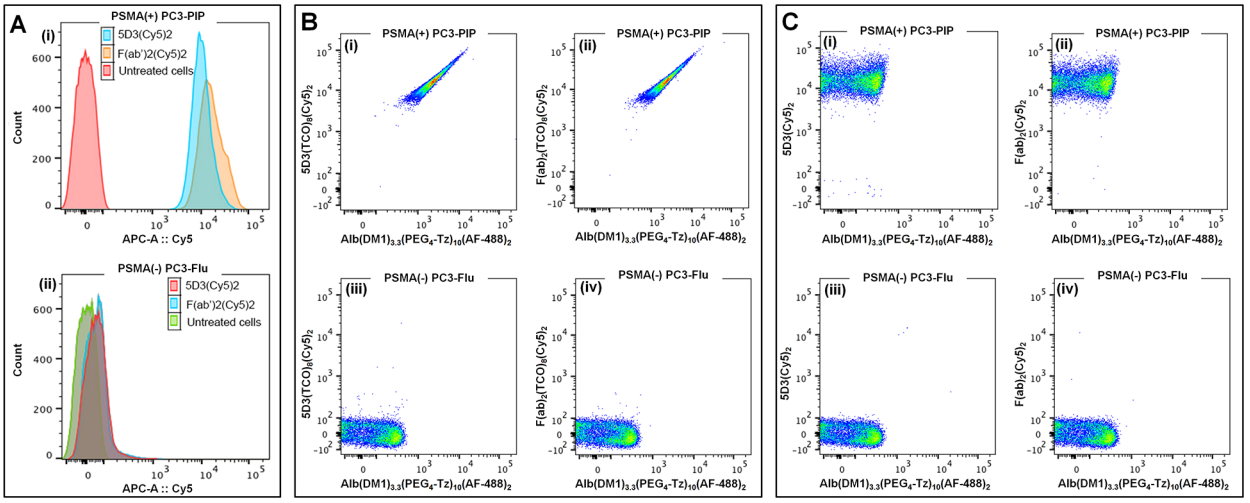

Figure 2. Flow cytometry analysis of the pretargeted click-chemistry delivery. (A) PSMA expression levels in (i) PC3-PIP and (ii) PC3-Flu cells. Combined histograms of untreated cells and cells treated with 5D3$(Cy5)_2$ and F(ab′$)_2(Cy5)_2$. (B) Pretargeted delivery in the presence of the click reaction between Alb$(DM1)_{3.3}(PEG_4\text{-}Tz)_{10}(AF\text{-}488)_2$ and reactive (i) 5D3$(TCO)_8(Cy5)_2$ in PC3-PIP cells, (ii) F(ab′$)_2(TCO)_8(Cy5)_2$ in PC3-PIP cells, (iii) 5D3$(TCO)_8(Cy5)_2$ in PC3-Flu cells, and (iv) F(ab′$)_2(TCO)_8(Cy5)_2$ in PC3-Flu cells. (C) Pretargeted delivery in the absence of a click reaction between ALB$(DM1)_{3.3}(PEG_4\text{-}Tz)_{10}(AF\text{-}488)_2$ and unreactive (i) 5D3$(Cy5)_2$ in PC3-PIP cells, (ii) F(ab′$)_2(Cy5)_2$ in PC3-PIP cells, (iii) 5D3$(Cy5)_2$ in PC3-Flu cells, and (iv) F(ab′$)_2(Cy5)_2$ in PC3-Flu cells.

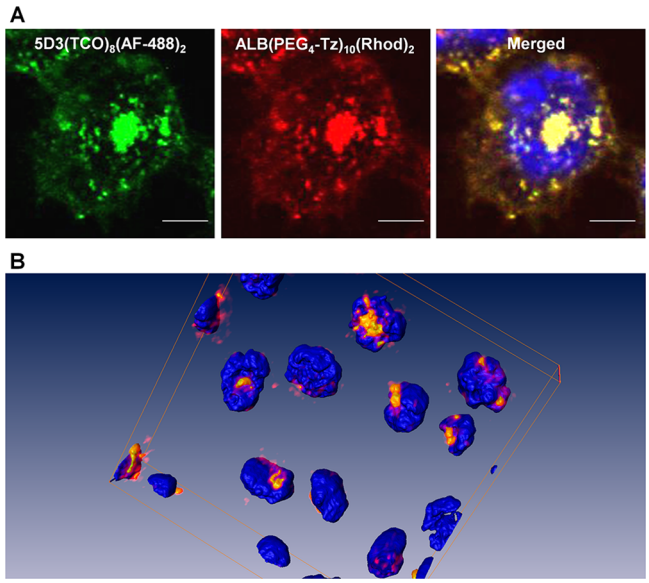

Figure 3. Fluorescence images of the pretargeted two-component delivery in PSMA(+) PC3-PIP cells, (A) using 5D3$(TCO)_8$(AF-$488)_2$ (green), ALB$(PEG_4\text{-}Tz)_{10}(Rhod)_2$ (red), and nuclear staining by Hoechst 33342 (blue) (magnification 100×, scale bar: 30 μm). (B) 3D rendering of the click therapy components colocalized in the cytoplasm of PSMA(+) cells.

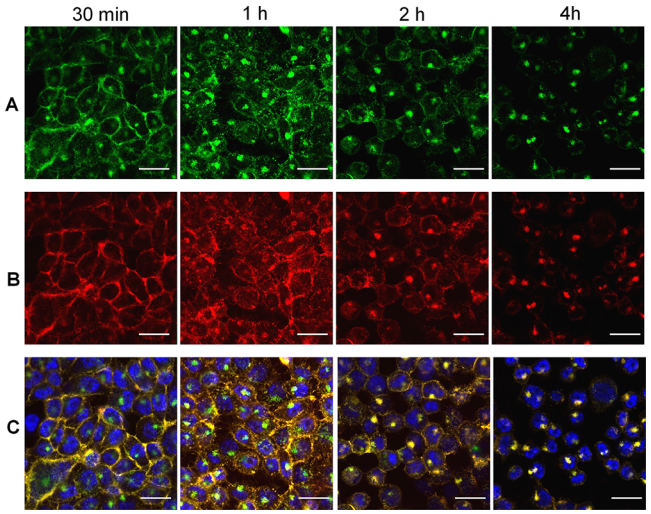

Figure 4. Time-dependent fluorescence images of PSMA(+) PC3-PIP cells in pretargeted drug delivery using 5D3$(TCO)_8$(AF-$488)_2$ and ALB$(DM1)_{3.3}(PEG_4\text{-}Tz)_{10}(Rhod)_2$. Panel A: Localization of the first component, 5D3$(TCO)_8$(AF-$488)_2$, over time after treatment with the drug delivery component (postdrug treatment time 30 min, 1, 2, 4 h). Panel B: Localization of the second drug delivery component, ALB$(DM1)_{3.3}(PEG_4\text{-}Tz)_{10}(Rhod)_2$, over time after the treatment (30 min, 1, 2, 4 h). Panel C: Merged images of corresponding green and red channels. (Scale bar: 100 μM.)

colocalization with the red channel. These free F(ab′$)_2(TCO)_8$ were internalized before *in situ* bioorthogonal click reactions with the drug delivery component.

3.6. Click Therapy on PSMA(±) Cells and Therapeutic Efficacy. PSMA(+) PC3-PIP and PSMA(−) PC3-Flu cells were treated following the therapeutic schedule shown in Table 1. First, four series of cell chambers were treated with 5D3$(TCO)_8$, F(ab′$)_2(TCO)_8$, unconjugated 5D3, or unconjugated F(ab′$)_2$, washed to remove excess pretargeting components, and subsequently treated with the drug delivery component, ALB$(DM1)_{3.3}(PEG_4\text{-}Tz)_{10}$. Next, four-cell chambers were treated with 5D3$(TCO)_8$, F(ab′$)_2(TCO)_8$, 5D3 mAb, or F(ab′$)_2$ fragments alone to evaluate the effect of pretargeting components on cell viability. Finally, two cell chambers were treated with ALB$(DM1)_{3.3}(PEG_4\text{-}Tz)_{10}$ or pure DM1 equiv of the DM1 concentration in ALB$(DM1)_{3.3}(PEG_4\text{-}Tz)_{10}$ to measure the effect of the drug or the drug carrier without the pretargeting paradigm.

As shown in Figure 8, the combination of 5D3$(TCO)_8$ and ALB$(DM1)_{3.3}(PEG_4\text{-}Tz)_{10}$ showed selective and enhanced toxicity in PSMA(+) PC3-PIP cells when compared to the combination of nonfunctionalized 5D3 and ALB-$(DM1)_{3.3}(PEG_4\text{-}Tz)_{10}$, or any other signal treatment compo-

DOI: 10.1021/acs.molpharmaceut.9b00788
Mol. Pharmaceutics 2020, 17, 98−108

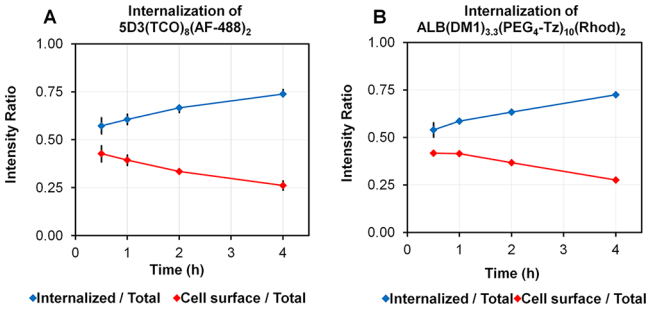

Figure 5. Change of the internalized and cell surface fluorescence intensity ratio of (A) $5D3(TCO)_8(AF\text{-}488)_2$ and (B) $ALB\text{-}(DM1)_{3.3}(PEG_4\text{-}Tz)_{10}(Rhod)_2$ with time.

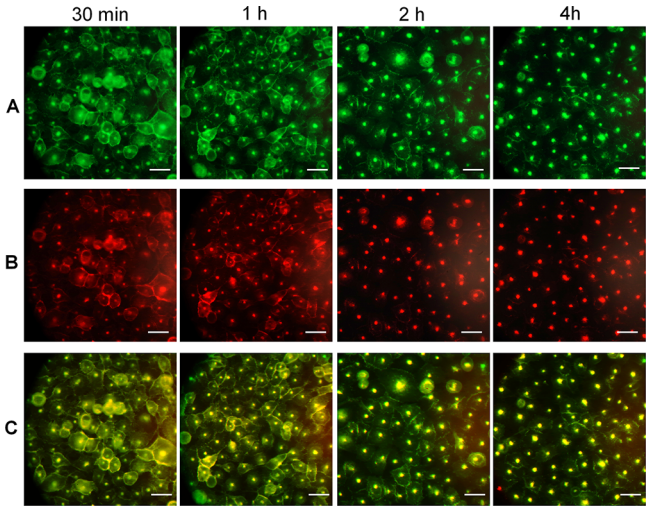

Figure 6. Time-dependent images of PSMA(+) PC3-PIP cells in pretargeted drug delivery using $F(ab')_2(TCO)_8(AF\text{-}488)_2$ and $ALB(DM1)_{3.3}(PEG_4\text{-}Tz)_{10}(Rhod)_2$. Panel A: Localization of the first component, $F(ab')_2(TCO)_8(AF\text{-}488)_2$, over the time after treatment with the drug delivery component (postdrug treatment time 30 min, 1, 2, 4 h). Panel B: Localization of the second drug delivery component, $ALB(DM1)_{3.3}(PEG_4\text{-}Tz)_{10}(Rhod)_2$, over the time after the treatment. Panel C: Merged images of corresponding green and red channels. (Scale bar: 100 μM.)

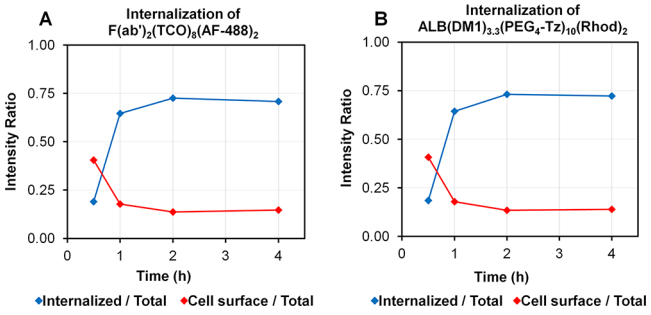

Figure 7. Change of the internalized and cell surface fluorescence intensity ratio of (A) $5D3\text{-}F(ab')_2(TCO)_8(AF\text{-}488)_2$ and (B) $ALB(DM1)_{3.3}(PEG_4\text{-}Tz)_{10}(Rhod)_2$ with time.

nent alone. This enhanced toxicity was not observed in PSMA(−) PC3-Flu cells, suggesting PSMA specificity. Surprisingly, the smaller $F(ab')_2$ fragments could not replicate this PSMA-specific toxicity. Click therapy using $5D_3(TCO)_8$ and $F(ab')_2(TCO)_8$ with $ALB(DM1)_{3.3}(PEG_4\text{-}Tz)_{10}$ as a drug delivery component exhibits a reduction of cell viability of 30%

Table 1. Click Therapy Treatment Schedule

Treat group	Pretargeting comp. (20 μg/mL, 130/180 nM)	Drug delivery comp. (50 μg/mL, 600 nM)
1	$5D3(TCO)_8$	$ALB(DM1)_{3.3}(PEG_4\text{-}Tz)_{10}$
2	$F(ab')_2(TCO)_8$	$ALB(DM1)_{3.3}(PEG_4\text{-}Tz)_{10}$
3	5D3	$ALB(DM1)_{3.3}(PEG_4\text{-}Tz)_{10}$
4	$F(ab')_2$	$ALB(DM1)_{3.3}(PEG_4\text{-}Tz)_{10}$
5	$5D3(TCO)_8$	
6	$F(ab')_2(TCO)_8$	
7	5D3	
8	$F(ab')_2$	
9		DM1 (2 μM)[a]
10		$ALB(DM1)_{3.3}(PEG_4\text{-}Tz)_{10}$

[a]The concentration of pure DM1 was equivalent for DM1 content in a drug delivery component.

and 55% of PSMA(+) PC3-PIP cells respectively, whereas the corresponding cell viabilities of PSMA(−) PC3-Flu cells were 49% and 40% when using $5D3(TCO)_8$ and $F(ab')_2(TCO)_8$ as pretargeting components, respectively. The therapeutic effect of the combination of $5D3(TCO)_8$ and $ALB(DM1)_{3.3}(PEG_4\text{-}Tz)_{10}$ was significantly higher compared to the treatment using $ALB(DM1)_{3.3}(PEG_4\text{-}Tz)_{10}$ alone and the nonclick combination of 5D3 mAb and $ALB(DM1)_{3.3}(PEG_4\text{-}Tz)_{10}$ in PC3-PIP cells. The treatment schedule of PSMA(−) PC3-Flu cells showed a significantly lower decrease in cell viability. Control experiments with $ALB(DM1)_{3.3}(PEG_4\text{-}Tz)_{10}$ and its equivalent DM1 treatment result in comparable 57% and 55% cell viabilities in PC3-PIP cells and 63% and 55% cell viabilities in PC3-Flu cells, respectively. The controlled, targeted two-component delivery without click conjugation using pure 5D3 and $F(ab')_2$ with $ALB(DM1)_{3.3}(PEG_4\text{-}Tz)_{10}$ reduces the cell viability to 48% and 52% in PC3-PIP cells and 45% to 42% in PC3-Flu cells; however, this is not significantly different compared to $ALB(DM1)_{3.3}(PEG_4\text{-}Tz)_{10}$ alone.

4. DISCUSSION

We selected anti-PSMA 5D3 as a pretargeting mAb due to its high binding affinity compared to other existing/commercially available anti-PSMA mAbs. Antibodies that have been used as imaging agents and drug carriers are biocompatible, and their intrinsic amine groups can be easily used for modification and conjugation purposes. Approximately eight TCO groups per mAb provide the optimal substitution ratio for receptor binding and multiple click reactions with the delivery component to produce cross-linked nanoclusters without interfering with the binding affinity.[45] Human serum albumin is used in the clinic, as the drug-carrier molecule (Abraxane),[54] and as a platform for the development of drug delivery components.[55,56] Albumin is a hydrophilic globular protein, which is highly stable in a broad pH range (pH 4−9), up to 40% ethanol, and temperature up to 60 °C. Albumin is also used as a drug carrier for delivery of hydrophobic low-molecular-weight chemotherapeutics in cancer therapy.[57,58]

We have used PC3-PIP and PC3-Flu cells in this study to validate the concept in PC. PSMA is highly overexpressed in PC3-PIP cells compared to PC3-Flu cells, as proven in Figure 2A. In our experiments, $F(ab')_2$ alone was internalized faster than 5D3 mAb (75% of 5D3 in 2.5 h vs 75% of $F(ab')_2$ in 1 h), presumably due to their small size and efficient cross-linking of PSMA receptors on the cell surface. However, the fast internalization is a disadvantage in pretargeted delivery since

DOI: 10.1021/acs.molpharmaceut.9b00788
Mol. Pharmaceutics 2020, 17, 98−108

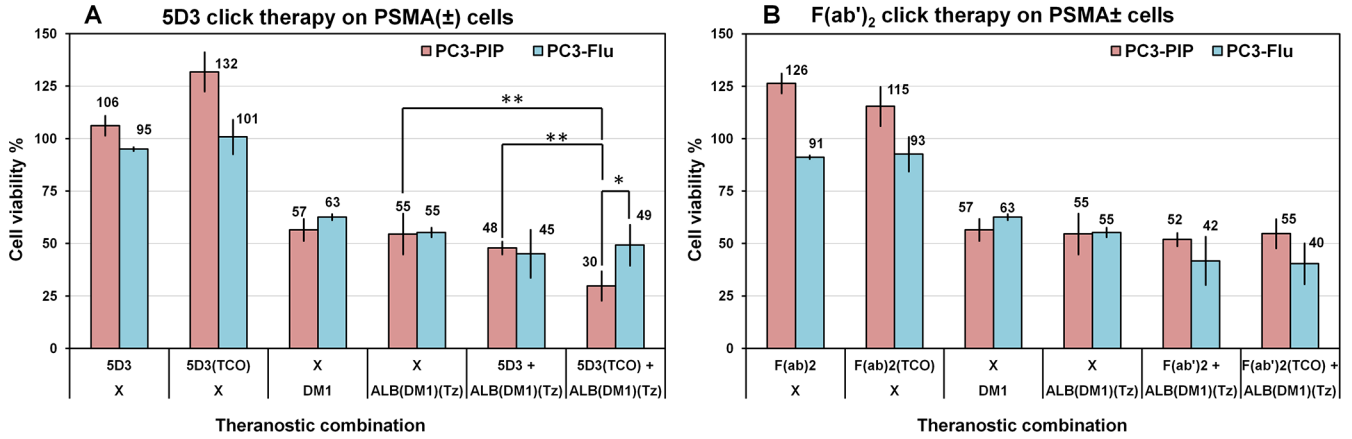

Figure 8. Cell viability-based *in vitro* therapeutic study of pretargeted two-component drug delivery. 5D3(TCO)$_8$ (A) and F(ab′)$_2$(TCO)$_8$ (B) were used as a pretargeting component. Control experiments were performed with the pretargeting component alone; pure DM1 or with ALB(DM1)$_{3.3}$(PEG$_4$-Tz)$_{10}$ without pretargeting components. The combination of 5D3(TCO)$_8$ and ALB(DM1)$_{3.3}$(PEG$_4$-Tz)$_{10}$ showed selective and enhanced toxicity in PSMA(+) PC3-PIP cells when compared to the combination of nonfunctionalized 5D3 and ALB(DM1)$_{3.3}$(PEG$_4$-Tz)$_{10}$ or treatment with a free drug or drug-carrier component alone. This enhanced toxicity was not observed in PSMA(−) PC3-Flu cells, suggesting PSMA specificity. PSMA-specific toxicity of the smaller F(ab′)$_2$ fragments, used as the pretargeting component, could not replicate this of complete 5D3 mAb (*p < 0.05, **p < 0.005).

the time window spent by the pretargeting component on the cell surface is critical for click reactions with the second drug delivery component. After internalization, the receptors could be recycled, and the pretargeting component was retained in the cytoplasm, rendering it unavailable for reaction with the drug carrier.

Next, we assessed the pretargeted delivery driven by TCO-Tz click chemistry in PSMA(+) PC3-PIP and PSMA(−) PC3-Flu cells. When the click delivery has taken place in PSMA(+) cells, the colocalized Cy5 and AF-488 fluorescence signals corresponding to 5D3(TCO)$_8$(Cy5)$_2$ or F(ab′)$_2$(TCO)$_8$(Cy5)$_2$ and ALB(DM1)$_{3.3}$(PEG$_4$-Tz)$_{10}$(AF-488)$_2$ are detected in each cell (Figure 2B); both fluorescence signals are higher in the FACS density plot. However, when nonreactive compounds are used, high fluorescence signals of the pretargeting components only are detected in PSMA(+) cells but not in PSMA(−) cells (Figure 2C). The pretargeting component 5D3(TCO)$_8$(AF-488)$_2$ labeled the cell surface PSMA receptors and stayed on the membrane for at least 30 min. The second-component, ALB(PEG$_4$-Tz)$_{10}$(Rhod)$_2$, undergoes multiple *in situ* TCO-Tz click reactions with the pretargeting components on the cell surface, making cross-linked nanoclusters, leading to their rapid internalization. Multiple functional groups (TCO or Tz) per component, the close proximity of PSMA receptors in PSMA(+) cell surface, and fast kinetics (~300 000 M^{-1} s^{-1}) of TCO-Tz click reaction facilitate the formation of nanoclusters of two components on the cell surface.[59] If solutions of both components (~10 mg/mL) are mixed at room temperature, the mixture rapidly becomes cloudy because of multiple click reactions between components and the formation of large protein−protein complexes.

The cross-linking is not feasible on cells with a low or absent expression of PSMA, and therefore, this strategy can be used to selectively deliver drugs to malignant cells. Pretargeted click therapy was further investigated by a time-dependent study of PC3-PIP cells using 5D3(TCO)$_8$(AF-488)$_2$ (Figure 4) and F(ab′)$_2$(TCO)$_8$(AF-488)$_2$ (Figure 6) with ALB-(DM1)$_{3.3}$(PEG$_4$-Tz)$_{10}$(Rhod)$_2$. In these studies, both components were colocalized on the cell surface. However, a significant amount of unconjugated or unreacted F-(ab′)$_2$(TCO)$_8$(AF-488)$_2$ was observed in endosomes in the cell cytoplasm, due to its fast internalization, and was not available for *in situ* click conjugation and the formation of nanoclusters.

In vitro therapeutic study reveals no reduction in cell viability by 5D3 mAb or its TCO conjugated analogues (Figure 8). However, treatment of PC3-PIP cells with ALB-(DM1)$_{3.3}$(PEG$_4$-Tz)$_{10}$ or its equivalent concentration of pure DM1 almost equally reduced cell viability. An efficient cross-linking of two components, 5D3(TCO)$_8$ and ALB-(DM1)$_{3.3}$(PEG$_4$-Tz)$_{10}$, on the targeted cell surface leads to enhanced cellular internalization and results in the highest therapeutic effects in PSMA(+) PC3-PIP cells compared to PSMA(−) PC3-Flu cells. Substituting the complete mAb with its F(ab′)$_2$ fragment as a pretargeting component does not enhance the therapeutic efficacy of ALB(DM1)$_{3.3}$(PEG$_4$-Tz)$_{10}$. Free DM1 is a highly cytotoxic molecule (IC_{50} in a low nanomolar range for most cancer cells)[60] and reduces cell viability to ~60% after 2 h incubation at a concentration of 2 μM. As a naturally abundant carrier and transporting protein in the blood, albumin is one of the most important proteins taken nonspecifically by cells. Hence, we observed the therapeutic effects of untargeted ALB(DM1)$_{3.3}$(PEG$_4$-Tz)$_{10}$(Rhod)$_2$ in both PC3-PIP and PC3-Flu cells. Interestingly, in the control study shown in Figure S4, we observe a minimal uptake of ALB(DM1)$_{3.3}$(PEG$_4$-Tz)$_{10}$(Rhod)$_2$ in PC3-PIP cells. For comparison, in similar experiments with HER2-positive and HER2-negative breast cancer cells and albumin−paclitaxel conjugates (paclitaxel IC_{50} = 2.5−7.5 nM),[61] we observed moderate cytotoxicity of the carrier, which reduced cell viability to ~70−75%.[45] Enhanced cell-kill effects of the free and albumin-bound DM1 even with limited uptake of the free form and albumin-bound drug after 2 h pulse treatment of cells can be attributed to the significantly higher cytotoxicity of the drug (IC_{50} = 1.1 nM).[60] We have also observed an enhancement (not statistically significant) of cell viability after pure 5D3, F(ab′)$_2$, and 5D3(TCO)$_8$, and F(ab′)$_2$(TCO)$_8$ treatment. It appeared to be a slight enhancement of cell growth by anti-PSMA agents, possibly due to interference with

DOI: 10.1021/acs.molpharmaceut.9b00788
Mol. Pharmaceutics 2020, 17, 98−108

signaling pathways in cells. As proven by the mAb and $F(ab')_2$ internalization study, fast internalization kinetics of the $F(ab')_2$ domain, and its small size, has diminished the efficient cross-linking with the drug delivery component and therefore resulted in the reduced efficacy.

Our previous study of HER2(+) breast cancer in orthotopic mouse models using anti-HER2 mAb, trastuzumab proved that this strategy can be successfully applied *in vivo* because HER2 receptors inherently exhibit poor internalization even after ligand binding. Ideally, internalization and pharmacokinetics of the pretargeting agent should have a similar time scale. In the case of PSMA receptors, both 5D3 mAb and its $F(ab')_2$ fragments have fast internalization rates, which may present a problem for *in vivo* applications. While the system provided an enhanced specific kill of PSMA(+) PC cells *in vitro*, the internalization kinetics of the pretargeting agent has been identified as a critical parameter, affecting the treatment efficacy. This will become an issue for *in vivo* applications, where the timing of administration of the drug-carrier component should be optimized based on pharmacokinetics and tumor accumulation of the pretargeting component. We envision that for successful translation of the technology *in vivo*, further advances in the design of pretargeting components with a relatively fast clearance time and sufficient persistence on the cellular membrane is required.

5. CONCLUSION

Based on our experimental results, the overall efficacy of the pretargeted approach critically depends on several factors: (1) efficient binding of the pretargeting moiety to the target receptor; (2) sufficient time on the cell surface before internalization to enable click chemistry cross-linking with the drug delivery component; (3) highly cytotoxic therapeutic cargo, such as the DM1 microtubulin inhibitor of microtubule polymerization. On the basis of encouraging results obtained *in vitro* experiments, we are currently extending our study to investigate strategies for delaying internalization and evaluate the therapeutic effects of the pretargeted strategy *in vivo* in mouse models of human PC.

■ ASSOCIATED CONTENT

Supporting Information

The Supporting Information is available free of charge at https://pubs.acs.org/doi/10.1021/acs.molpharmaceut.9b00788.

MALDI-TOF analysis of components, dynamic light scattering (DLS) analysis of components, internalization of anti-PSMA 5D3 mAb and $F(ab')_2$, and imaging experiment with $ALB(PEG_4\text{-}Tz)_{10}(Rhod)_2$ (PDF)

■ AUTHOR INFORMATION

Corresponding Authors

*E-mail:shapuar1@jhmi.edu. Phone: +1(443) 287-4426. Fax: +1(410) 614-1948.

*E-mail: dartemo2@jhmi.edu. Phone: +1(410) 614-2703. Fax: +1(410) 614-1948.

ORCID

Sudath Hapuarachchige: 0000-0002-1166-8247

Cyril Bařinka: 0000-0003-2751-3060

Martin G. Pomper: 0000-0001-6753-3010

Notes

The authors declare no competing financial interest.

■ ACKNOWLEDGMENTS

This study was supported by the Department of Defense (DoD) grant (W81XWH-16-1-0595), Czech Science Foundation grant (18-04790S), the European Regional Development Fund (Project BIOCEV-CZ.1.05/1.1.00/02.0109), and Czech Academy of Sciences grant (RVO: 86652036). This work also partially supported by R01 grants (CA209884, CA134675, and CA184228) from the National Cancer Institute, grant (EB024495) from the Institute National Institute of Biomedical Imaging and Bioengineering, National Institutes of Health, and Emerson Collective grant (128821) from Emerson Collective Cancer Research Fund. The authors acknowledge Dixie Hoyle for her assistance in flow cytometry.

■ ABBREVIATIONS

ADC, antibody−drug conjugate; ALB, human serum albumin; DM1, mertansine; DPBS, Dulbecco's phosphate buffered saline; HPLC, high-performance liquid chromatography; IEDDA, inverse-electron demand Diels−Alder; mAb, monoclonal antibody; MALDI-TOF, matrix-assisted laser desorption ionization time-of-flight mass spectrometry; PBS, BupH phosphate buffered saline; PC, prostate cancer; PSMA, prostate-specific membrane antigen; SEC, size-exclusion chromatography; Sulfo-SMCC, sulfosuccinimidyl 4-(*N*-maleimiddomethyl)cyclohexane-1-carboxylate; TCO, *trans*-cyclooctene; Tz, tetrazine

■ REFERENCES

(1) Reddy, A.; Roberts, R.; Shenoy, D.; Packianathan, S.; Giri, S.; Vijayakumar, S. Prostate Cancer Screening Guidelines for African American Veterans: A New Perspective. *J. Natl. Med. Assoc.* **2018**.

(2) Ahlborg, H.; Nightingale, A. J. Mismatch between Scales of Knowledge in Nepalese Forestry: Epistemology, Power, and Policy Implications. *Ecology and Society* **2012**, *17*, 1.

(3) Siegel, R. L.; Miller, K. D.; Jemal, A. Cancer Statistics, 2019. *Ca-Cancer J. Clin.* **2019**, *69*, 7−34.

(4) Fang, J. C.; Faerber, G.; Samadder, J. Digital Rectal Examination for Prostate Cancer Screening Performed with Colonoscopy for Colon Cancer Screening: 2 for the Price of 1. *Gastrointestinal Endoscopy* **2017**, *86*, 1147−1150.

(5) Zerbib, M.; Zelefsky, M. J.; Higano, C. S.; Carroll, P. R. Conventional Treatments of Localized Prostate Cancer. *Urology* **2008**, *72*, 25−35.

(6) Frieling, J. S.; Basanta, D.; Lynch, C. C. Current and Emerging Therapies for Bone Metastatic Castration-Resistant Prostate Cancer. *Cancer Control* **2015**, *22*, 109−120.

(7) Gaya, J. M.; Huguet, J.; Breda, A.; Palou, J. [Surgical Treatment of Local Disease in Metastatic Prostate Cancer.]. *Arch Esp Urol* **2018**, *71*, 288−297.

(8) Vanneste, B. G.; Van Limbergen, E. J.; van Lin, E. N.; van Roermund, J. G.; Lambin, P. Prostate Cancer Radiation Therapy: What Do Clinicians Have to Know? *BioMed Res. Int.* **2016**, *2016*, 6829875.

(9) Das, M. Androgen Deprivation Therapy for Prostate Cancer. *Lancet Oncol.* **2017**, *18*, e567.

(10) Sartor, O.; de Bono, J. S. Metastatic Prostate Cancer. *N. Engl. J. Med.* **2018**, *378*, 1653−1654.

(11) Lee, C. H.; Kantoff, P. Treatment of Metastatic Prostate Cancer in 2018. *JAMA Oncol* **2019**, *5*, 263.

(12) Osanto, S.; Van Poppel, H. Emerging Novel Therapies for Advanced Prostate Cancer. *Ther. Adv. Urol.* **2012**, *4*, 3−12.

DOI: 10.1021/acs.molpharmaceut.9b00788
Mol. Pharmaceutics 2020, 17, 98−108

(13) Clarke, J. M.; Armstrong, A. J. Novel Therapies for the Treatment of Advanced Prostate Cancer. *Curr. Treat Options Oncol* **2013**, *14*, 109−126.
(14) Poon, D. M.; Ng, J.; Chan, K. Importance of Cycles of Chemotherapy and Postdocetaxel Novel Therapies in Metastatic Castration-Resistant Prostate Cancer. *Prostate Int.* **2015**, *3*, 51−55.
(15) Bouchelouche, K.; Choyke, P. L.; Capala, J. Prostate Specific Membrane Antigen - a Target for Imaging and Therapy with Radionuclides. *Discovery Medicine* **2010**, *9*, 55−61.
(16) Bravaccini, S.; Puccetti, M.; Bocchini, M.; Ravaioli, S.; Celli, M.; Scarpi, E.; De Giorgi, U.; Tumedei, M. M.; Raulli, G.; Cardinale, L. Psma Expression: A Potential Ally for the Pathologist in Prostate Cancer Diagnosis. *Sci. Rep.* **2018**, *8*, 1.
(17) Mease, R. C.; Foss, C. A.; Pomper, M. G. Pet Imaging in Prostate Cancer: Focus on Prostate-Specific Membrane Antigen. *Curr. Top. Med. Chem.* **2013**, *13*, 951−962.
(18) Chatalic, K. L. S.; Veldhoven-Zweistra, J.; Bolkestein, M.; Hoeben, S.; Koning, G. A.; Boerman, O. C.; de Jong, M.; van Weerden, W. M. A Novel in-111-Labeled Anti-Prostate-Specific Membrane Antigen Nanobody for Targeted Spect/Ct Imaging of Prostate Cancer. *J. Nucl. Med.* **2015**, *56*, 1094−1099.
(19) Chang, S. S. Overview of Prostate-Specific Membrane Antigen. *Rev. Urol* **2004**, *6 Suppl 10*, S13−18.
(20) Langut, Y.; Talhami, A.; Mamidi, S.; Shir, A.; Zigler, M.; Joubran, S.; Sagalov, A.; Flashner-Abramson, E.; Edinger, N.; Klein, S.; et al. Psma-Targeted Polyinosine/Polycytosine Vector Induces Prostate Tumor Regression and Invokes an Antitumor Immune Response in Mice. *Proc. Natl. Acad. Sci. U. S. A.* **2017**, *114*, 13655−13660.
(21) Wustemann, T.; Haberkorn, U.; Babich, J.; Mier, W. Targeting Prostate Cancer: Prostate-Specific Membrane Antigen Based Diagnosis and Therapy. *Med. Res. Rev.* **2019**, *39*, 40−69.
(22) Yao, V.; Berkman, C. E.; Choi, J. K.; O'Keefe, D. S.; Bacich, D. J. Expression of Prostate-Specific Membrane Antigen (Psma), Increases Cell Folate Uptake and Proliferation and Suggests a Novel Role for Psma in the Uptake of the Non-Polyglutamated Folate, Folic Acid. *Prostate* **2009**, *70*, 305−316.
(23) Mesters, J. R.; Barinka, C.; Li, W.; Tsukamoto, T.; Majer, P.; Slusher, B. S.; Konvalinka, J.; Hilgenfeld, R. Structure of Glutamate Carboxypeptidase Ii, a Drug Target in Neuronal Damage and Prostate Cancer. *EMBO J.* **2006**, *25*, 1375−1384.
(24) Barinka, C.; Rojas, C.; Slusher, B.; Pomper, M. Glutamate Carboxypeptidase Ii in Diagnosis and Treatment of Neurologic Disorders and Prostate Cancer. *Curr. Med. Chem.* **2012**, *19*, 856−870.
(25) Pinto, J. T.; Suffoletto, B. P.; Berzin, T. M.; Qiao, C. H.; Lin, S.; Tong, W. P.; May, F.; Mukherjee, B.; Heston, W. D. Prostate-Specific Membrane Antigen: A Novel Folate Hydrolase in Human Prostatic Carcinoma Cells. *Clin. Cancer Res.* **1996**, *2*, 1445−1451.
(26) Carter, R. E.; Feldman, A. R.; Coyle, J. T. Prostate-Specific Membrane Antigen Is a Hydrolase with Substrate and Pharmacologic Characteristics of a Neuropeptidase. *Proc. Natl. Acad. Sci. U. S. A.* **1996**, *93*, 749−753.
(27) Rahbar, K.; Afshar-Oromieh, A.; Jadvar, H.; Ahmadzadehfar, H. Psma Theranostics: Current Status and Future Directions. *Mol. Imaging* **2018**, *17*, 153601211877606.
(28) Azad, B. B.; Banerjee, S. R.; Pullambhatla, M.; Lacerda, S.; Foss, C. A.; Wang, Y. C.; Ivkov, R.; Pomper, M. G. Evaluation of a Psma-Targeted Bnf Nanoparticle Construct. *Nanoscale* **2015**, *7*, 4432−4442.
(29) Chandran, S. S.; Banerjee, S. R.; Mease, R. C.; Pomper, M. G.; Denmeade, S. R. Characterization of a Targeted Nanoparticle Functionalized with a Urea-Based Inhibitor of Prostate-Specific Membrane Antigen (Psma). *Cancer Biol. Ther.* **2008**, *7*, 974−982.
(30) Jin, W.; Qin, B.; Chen, Z. J.; Liu, H.; Barve, A.; Cheng, K. Discovery of Psma-Specific Peptide Ligands for Targeted Drug Delivery. *Int. J. Pharm.* **2016**, *513*, 138−147.
(31) Liu, T. C.; Nedrow-Byers, J. R.; Hopkins, M. R.; Wu, L. S. Y.; Lee, J.; Reilly, P. T. A.; Berkman, C. E. Targeting Prostate Cancer Cells with a Multivalent Psma Inhibitor-Guided Streptavidin Conjugate. *Bioorg. Med. Chem. Lett.* **2012**, *22*, 3931−3934.
(32) Fuchs, A. V.; Tse, B. W.; Pearce, A. K.; Yeh, M. C.; Fletcher, N. L.; Huang, S. S.; Heston, W. D.; Whittaker, A. K.; Russell, P. J.; Thurecht, K. J. Evaluation of Polymeric Nanomedicines Targeted to Psma: Effect of Ligand on Targeting Efficiency. *Biomacromolecules* **2015**, *16*, 3235−3247.
(33) Liu, H.; Rajasekaran, A. K.; Moy, P.; Xia, Y.; Kim, S.; Navarro, V.; Rahmati, R.; Bander, N. H. Constitutive and Antibody-Induced Internalization of Prostate-Specific Membrane Antigen. *Cancer Res.* **1998**, *58*, 4055−4060.
(34) Tagawa, S. T.; Milowsky, M. I.; Morris, M.; Vallabhajosula, S.; Christos, P.; Akhtar, N. H.; Osborne, J.; Goldsmith, S. J.; Larson, S.; Taskar, N. P.; et al. Phase Ii Study of Lutetium-177-Labeled Anti-Prostate-Specific Membrane Antigen Monoclonal Antibody J591 for Metastatic Castration-Resistant Prostate Cancer. *Clin. Cancer Res.* **2013**, *19*, 5182−5191.
(35) Tagawa, S. T.; Milowsky, M. I.; Morris, M. J.; Vallabhajosula, S.; Goldsmith, S.; Matulich, D.; Kaplan, J.; Berger, F.; Scher, H. I.; Bander, N. H. Phase Ii Trial of 177lutetium Radiolabeled Anti-Prostate-Specific Membrane Antigen (Psma) Monoclonal Antibody J591 (177lu-J591) in Patients (Pts) with Metastatic Castrate-Resistant Prostate Cancer (Metcrpc). *J. Clin. Oncol.* **2008**, *26*, 5140.
(36) Han, D. H.; Wu, J. H.; Han, Y. H.; Wei, M.; Han, S.; Lin, R. H.; Sun, Z. Y.; Yang, F.; Jiao, D.; Xie, P.; et al. A Novel Anti-Psma Human Scfv Has the Potential to Be Used as a Diagnostic Tool in Prostate Cancer. *Oncotarget* **2016**, *7*, 59471−59481.
(37) Novakova, Z.; Foss, C. A.; Copeland, B. T.; Morath, V.; Baranova, P.; Havlinova, B.; Skerra, A.; Pomper, M. G.; Barinka, C. Novel Monoclonal Antibodies Recognizing Human Prostate-Specific Membrane Antigen (Psma) as Research and Theranostic Tools. *Prostate* **2017**, *77*, 749−764.
(38) Ray Banerejee, S.; Kumar, V.; Lisok, A.; Plyku, D.; Novakova, Z.; Wharram, B.; Brummet, M.; Barinka, C.; Hobbs, R. F.; Pomper, M. G. Evaluation of (111)in-Dota-5d3, a Surrogate Spect Imaging Agent for Radioimmunotherapy of Prostate-Specific Membrane Antigen. *J. Nucl. Med.* **2019**, *60*, 400.
(39) Beck, A.; Goetsch, L.; Dumontet, C.; Corvaia, N. Strategies and Challenges for the Next Generation of Antibody Drug Conjugates. *Nat. Rev. Drug Discovery* **2017**, *16*, 315−337.
(40) Lyon, R. Drawing Lessons from the Clinical Development of Antibody-Drug Conjugates. *Drug Discovery Today: Technol.* **2018**, *30*, 105−109.
(41) Nicolaou, K. C.; Rigol, S. Total Synthesis in Search of Potent Antibody-Drug Conjugate Payloads. From the Fundamentals to the Translational. *Acc. Chem. Res.* **2019**, *52*, 127.
(42) Diamantis, N.; Banerji, U. Antibody-Drug Conjugates-an Emerging Class of Cancer Treatment. *Br. J. Cancer* **2016**, *114*, 362−367.
(43) Bae, Y. H.; Park, K. Targeted Drug Delivery to Tumors: Myths, Reality and Possibility. *J. Controlled Release* **2011**, *153*, 198−205.
(44) Hapuarachchige, S.; Kato, Y.; Artemov, D. Bioorthogonal Two-Component Drug Delivery in Her2(+) Breast Cancer Mouse Models. *Sci. Rep.* **2016**, *6*, 1.
(45) Hapuarachchige, S.; Zhu, W.; Kato, Y.; Artemov, D. Bioorthogonal, Two-Component Delivery Systems Based on Antibody and Drug-Loaded Nanocarriers for Enhanced Internalization of Nanotherapeutics. *Biomaterials* **2014**, *35*, 2346−2354.
(46) McKay, C. S.; Finn, M. G. Click Chemistry in Complex Mixtures: Bioorthogonal Bioconjugation. *Chem. Biol.* **2014**, *21*, 1075−1101.
(47) Karver, M. R.; Weissleder, R.; Hilderbrand, S. A. Bioorthogonal Reaction Pairs Enable Simultaneous, Selective, Multi-Target Imaging. *Angew. Chem., Int. Ed.* **2012**, *51*, 920−922.
(48) Chen, Z.; Krishnamachary, B.; Penet, M. F.; Bhujwalla, Z. M. Acid-Degradable Dextran as an Image Guided Sirna Carrier for Cox-2 Downregulation. *Theranostics* **2018**, *8*, 1−12.
(49) Liu, J.; Kopeckova, P.; Buhler, P.; Wolf, P.; Pan, H.; Bauer, H.; Elsasser-Beile, U.; Kopecek, J. Biorecognition and Subcellular Trafficking of Hpma Copolymer-Anti-Psma Antibody Conjugates by Prostate Cancer Cells. *Mol. Pharmaceutics* **2009**, *6*, 959−970.

DOI: 10.1021/acs.molpharmaceut.9b00788
Mol. Pharmaceutics 2020, 17, 98−108

(50) Vercauteren, D.; Vandenbroucke, R. E.; Jones, A. T.; Rejman, J.; Demeester, J.; De Smedt, S. C.; Sanders, N. N.; Braeckmans, K. The Use of Inhibitors to Study Endocytic Pathways of Gene Carriers: Optimization and Pitfalls. *Mol. Ther.* **2010**, *18*, 561−569.
(51) Shang, L.; Nienhaus, K.; Nienhaus, G. U. Engineered Nanoparticles Interacting with Cells: Size Matters. *J. Nanobiotechnol.* **2014**, *12*, 5.
(52) Yameen, B.; Choi, W. I.; Vilos, C.; Swami, A.; Shi, J. J.; Farokhzad, O. C. Insight into Nanoparticle Cellular Uptake and Intracellular Targeting. *J. Controlled Release* **2014**, *190*, 485−499.
(53) Zhu, W.; Okollie, B.; Artemov, D. Controlled Internalization of Her-2/ Neu Receptors by Cross-Linking for Targeted Delivery. *Cancer Biol. Ther.* **2007**, *6*, 1960−1966.
(54) Kundranda, M. N.; Niu, J. Albumin-Bound Paclitaxel in Solid Tumors: Clinical Development and Future Directions. *Drug Des., Dev. Ther.* **2015**, *9*, 3767−3777.
(55) Rabbani, G.; Ahn, S. N. Structure, Enzymatic Activities, Glycation and Therapeutic Potential of Human Serum Albumin: A Natural Cargo. *Int. J. Biol. Macromol.* **2019**, *123*, 979−990.
(56) Karimi, M.; Bahrami, S.; Ravari, S. B.; Zangabad, P. S.; Mirshekari, H.; Bozorgomid, M.; Shahreza, S.; Sori, M.; Hamblin, M. R. Albumin Nanostructures as Advanced Drug Delivery Systems. *Expert Opin. Drug Delivery* **2016**, *13*, 1609−1623.
(57) Larsen, M. T.; Kuhlmann, M.; Hvam, M. L.; Howard, K. A. Albumin-Based Drug Delivery: Harnessing Nature to Cure Disease. *Mol. Cell Ther* **2016**, *4*, 3.
(58) Umbricht, C. A.; Benesova, M.; Schibli, R.; Muller, C. Preclinical Development of Novel Psma-Targeting Radioligands: Modulation of Albumin-Binding Properties to Improve Prostate Cancer Therapy. *Mol. Pharmaceutics* **2018**, *15*, 2297−2306.
(59) Darko, A.; Wallace, S.; Dmitrenko, O.; Machovina, M. M.; Mehl, R. A.; Chin, J. W.; Fox, J. M. Conformationally Strained Trans-Cyclooctene with Improved Stability and Excellent Reactivity in Tetrazine Ligation. *Chem. Sci.* **2014**, *5*, 3770−3776.
(60) Widdison, W. C.; Wilhelm, S. D.; Cavanagh, E. E.; Whiteman, K. R.; Leece, B. A.; Kovtun, Y.; Goldmacher, V. S.; Xie, H.; Steeves, R. M.; Lutz, R. J.; et al. Semisynthetic Maytansine Analogues for the Targeted Treatment of Cancer. *J. Med. Chem.* **2006**, *49*, 4392−4408.
(61) Liebmann, J. E.; Cook, J. A.; Lipschultz, C.; Teague, D.; Fisher, J.; Mitchell, J. B. Cytotoxic Studies of Paclitaxel (Taxol) in Human Tumour Cell Lines. *Br. J. Cancer* **1993**, *68*, 1104−1109.

DOI: 10.1021/acs.molpharmaceut.9b00788
Mol. Pharmaceutics 2020, 17, 98−108